Cell

RNA recoding in cephalopods tailors microtubule motor protein function

Graphical abstract

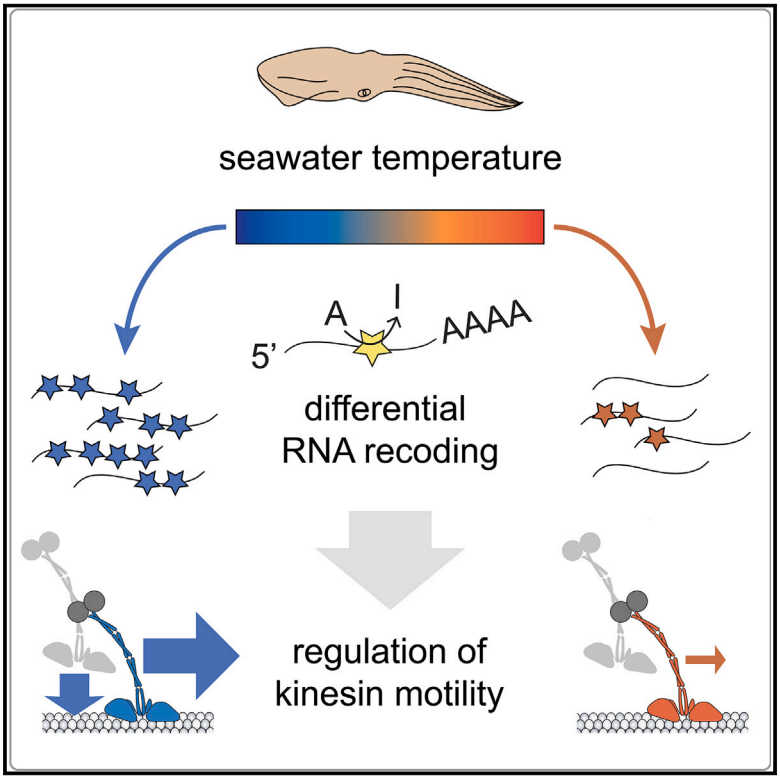

Highlights

- RNA editing in squid specifies unique kinesin protein variants in different tissues
- Unique kinesin variants are made acutely in response to seawater temperature
- Cold-specific kinesin variants have enhanced single molecule motility in the cold
- Cephalopod editomes can reveal functional substitutions in non-cephalopod proteins

Authors

Kavita J. Rangan,
Samara L. Reck-Peterson

Correspondence

krangan@health.ucsd.edu (K.J.R.),
sreckpeterson@health.ucsd.edu
(S.L.R.-P.)

In brief

RNA recoding in squid specifies unique kinesin variants with distinct activities in different tissues and in response to changes in seawater temperature, and cephalopod recoding sites provide a guide to identifying functional substitutions in non-cephalopod motor proteins.

Rangan & Reck-Peterson, 2023, Cell *186*, 2531–2543
June 8, 2023
https://doi.org/10.1016/j.cell.2023.04.032

CellPress

Cell

CellPress
OPEN ACCESS

Article

RNA recoding in cephalopods tailors microtubule motor protein function

Kavita J. Rangan[1,2,*] and Samara L. Reck-Peterson[1,2,3,4,*]
[1]Howard Hughes Medical Institute, Chevy Chase, MD 20815, USA
[2]Department of Cellular and Molecular Medicine, University of California San Diego, La Jolla, CA 92093, USA
[3]Department of Cell and Developmental Biology, University of California San Diego, La Jolla, CA 92093, USA
[4]Lead contact
*Correspondence: krangan@health.ucsd.edu (K.J.R.), sreckpeterson@health.ucsd.edu (S.L.R.-P.)
https://doi.org/10.1016/j.cell.2023.04.032

SUMMARY

RNA editing is a widespread epigenetic process that can alter the amino acid sequence of proteins, termed "recoding." In cephalopods, most transcripts are recoded, and recoding is hypothesized to be an adaptive strategy to generate phenotypic plasticity. However, how animals use RNA recoding dynamically is largely unexplored. We investigated the function of cephalopod RNA recoding in the microtubule motor proteins kinesin and dynein. We found that squid rapidly employ RNA recoding in response to changes in ocean temperature, and kinesin variants generated in cold seawater displayed enhanced motile properties in single-molecule experiments conducted in the cold. We also identified tissue-specific recoded squid kinesin variants that displayed distinct motile properties. Finally, we showed that cephalopod recoding sites can guide the discovery of functional substitutions in non-cephalopod kinesin and dynein. Thus, RNA recoding is a dynamic mechanism that generates phenotypic plasticity in cephalopods and can inform the characterization of conserved non-cephalopod proteins.

INTRODUCTION

Adenosine to inosine (A-to-I) RNA editing occurs widely across animals and serves many functions, including the regulation and diversification of mRNAs.[1] This type of editing is mediated by adenosine deaminase acting on RNA (ADAR) enzymes.[1] RNA editing in coding regions can generate non-synonymous codon changes, termed "recoding," which results in protein variants with altered amino acid composition.[2,3] In most animals, recoding through RNA editing is relatively rare; for example, recoding constitutes less than 1% of all reported editing sites in humans.[2] In contrast, RNA recoding occurs extensively in soft-bodied cephalopods[4]: ~60% of all mRNAs are recoded in squid, octopus, and cuttlefish.[5–8] RNA sequencing has revealed tens of thousands of recoding sites across the transcriptomes of these animals, and most recoded transcripts harbor multiple recoding sites. RNA recoding in cephalopods therefore has the potential to dramatically diversify the proteome.

Bioinformatic analyses of cephalopod RNA editing have led to a debate about the adaptive role and broad utility of recoding in these animals.[7,9,10] Sites of recoding display features of positive selection,[7,9,10] but the functional effects of recoding have only been assessed for a few cephalopod proteins, and most of this work has focused on voltage-gated potassium channels,[5,11–14] which are also recoded in mammals.[15] Outside of these proteins, the functional scope of cephalopod RNA recoding has not been explored.

It is hypothesized that cephalopods may use RNA recoding to dynamically modulate protein function in response to specific cellular[16] and environmental cues.[11,17] Indeed, RNA editing varies across different cephalopod species and tissues,[5–8,16] but it is not known if RNA recoding within these animals generates functionally distinct protein variants in response to environmental cues. For example, the frequency of recoding of the Kv1 potassium channel varies in different species of octopus that inhabit different climates,[11] but it is not known if RNA recoding within the same species can respond acutely and flexibly to changes in environmental temperature to alter protein function.

Many cephalopod recoding sites occur in uncharacterized amino acid residues that are widely conserved across other organisms, raising the possibility that cephalopod recoding sites could be harnessed as a unique map to reveal functional residues or targets of modulation in non-cephalopod proteins. This approach would be fundamentally different from conventional screening approaches, as recoding site substitutions may represent natural variants that animals employ to enhance or modulate protein function in different contexts. To evaluate this idea, we first needed to determine if RNA recoding can modulate protein function in cephalopods under different conditions and also determine if individual cephalopod recoding site substitutions can alter protein function in non-cephalopod protein homologs.

Here, we set out to investigate the function of cephalopod recoding in the microtubule motor proteins kinesin and dynein. First, we wanted to determine if RNA recoding is used as a

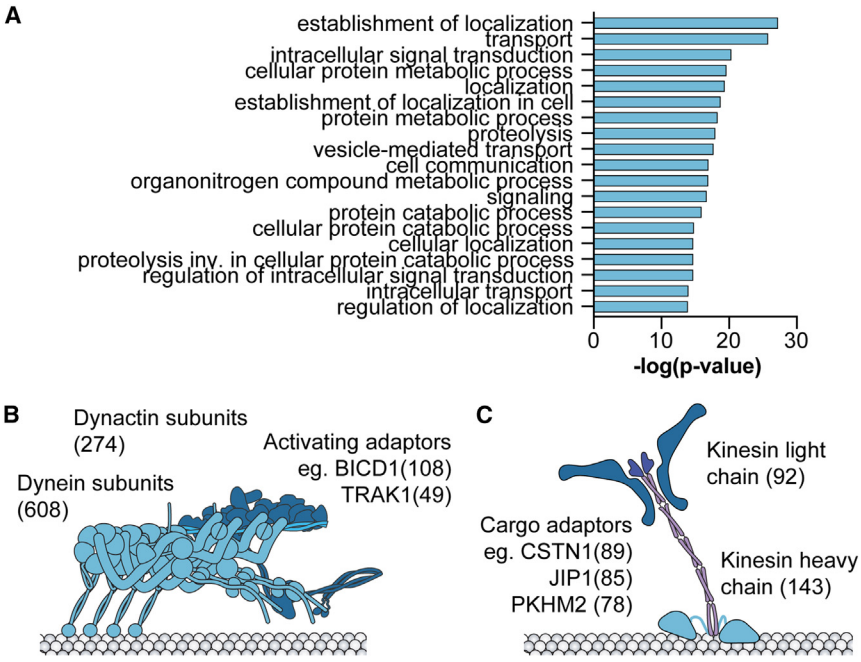

Figure 1. Microtubule motor proteins are a good model for exploring the function of cephalopod recoding

(A) Top 20 GO terms (biological process) significantly enriched amongst *D. pealeii* edited transcripts as compared to the full *D. pealeii* transcriptome. -$\log_{10}$ (p value) is shown and p values were determined by Fisher's exact t test.

(B and C) Sum of recoding sites reported by Liscovitch-Brauer et al. from *D. pealeii*, *S. officinalis*, *O. bimaculoides*, and *O. vulgaris* across dynein transport complex proteins (B) and kinesin transport complex proteins (C).

See also Table S1.

flexible mechanism for generating phenotypic plasticity within animals. We evaluated RNA recoding of squid kinesin and found that squid dynamically employ RNA recoding to generate unique kinesin variants in different tissues and in response to changes in ocean temperature, a relevant environmental factor for these animals. We then investigated how differential recoding in distinct tissues and environmental conditions altered the motile properties of squid kinesin. Using single-molecule experiments with recombinant squid kinesin, we found that kinesin variants generated in different tissues and different seawater temperatures displayed altered motile properties. This indicates that RNA recoding in cephalopods is responsive to environmental cues and may be used to support physiological needs by dynamically generating protein variants with tailored functions. Second, we wanted to determine if cephalopod recoding sites could reveal uncharacterized residues of functional significance in conserved non-cephalopod proteins. We assessed the functional effects of cephalopod recoding site substitutions in conserved residues within human kinesin and yeast dynein. Using this approach, we identified numerous unexpected substitutions in both kinesin and dynein that modulated motility, indicating that cephalopod recoding sites can be used to interrogate the function of conserved proteins.

RESULTS

Microtubule motors proteins are extensively recoded in cephalopods

Gene ontology (GO) term analysis of edited and unedited proteins from the longfin inshore squid, *Doryteuthis pealeii,* revealed that proteins involved in transport and localization are significantly enriched amongst edited proteins[5] (Figure 1A). Across cephalopods, proteins involved in microtubule-based transport are extensively recoded[5] (Figures 1B and 1C; Table S1). Cytoplasmic dynein-1 (*DYNC1H1* encodes the dynein heavy chain in humans, "dynein" here) and kinesin-1 (*KIF5B* in humans, "kinesin" here) are ideal model proteins to characterize the effects of recoding on protein function. Both dynein and kinesin are highly conserved and are structurally and mechanistically well characterized. In addition, single-molecule motility assays offer a robust method to quantify the effects of recoding on protein function (Figure S1).

Tissue-specific recoding alters squid kinesin motility

If RNA recoding is a mechanism for generating phenotypic plasticity, then differential recoding would be expected to generate protein variants with distinct functions in different tissues or environmental conditions. We focused on RNA recoding of kinesin-1 from the squid genus *Doryteuthis.* We first asked how squid kinesin is differentially recoded in different tissues. RNA sequencing has identified 37 recoding sites across 31 amino acids in the kinesin motor domain of *D. pealeii*[5–8] (Figure 2A), but it is unknown how these sites exist in combination along individual kinesin transcripts. We compared RNA recoding of the kinesin motor domain in two different squid neuronal cell populations: the stellate ganglion and the optic lobe (Figure 2B). The stellate ganglion includes the cluster of cell bodies that form the giant axon, which may necessitate distinct motor protein functions for rapid long-distance transport. To identify what kinesin variants are generated in each tissue, we extracted RNA from the stellate ganglion and the optic lobe and then sequenced individual cDNA clones of the kinesin motor domain from each tissue (Figure S2). Transcripts from the stellate ganglion were more extensively recoded compared to the optic lobe (Figure 2C), and we identified recoding site combinations that were unique to each tissue (Figure 2D). In both tissues, we detected more multiply recoded transcripts than would be expected if each site were edited independently. We detected significant pairwise correlations between recoding sites, and some of these correlations were tissue specific (Figures 2E and 2F). These data indicate that RNA recoding occurs in unique combinations in different tissues to generate tissue-specific kinesin protein variants and suggests tissue-specific regulation of combinatorial editing.

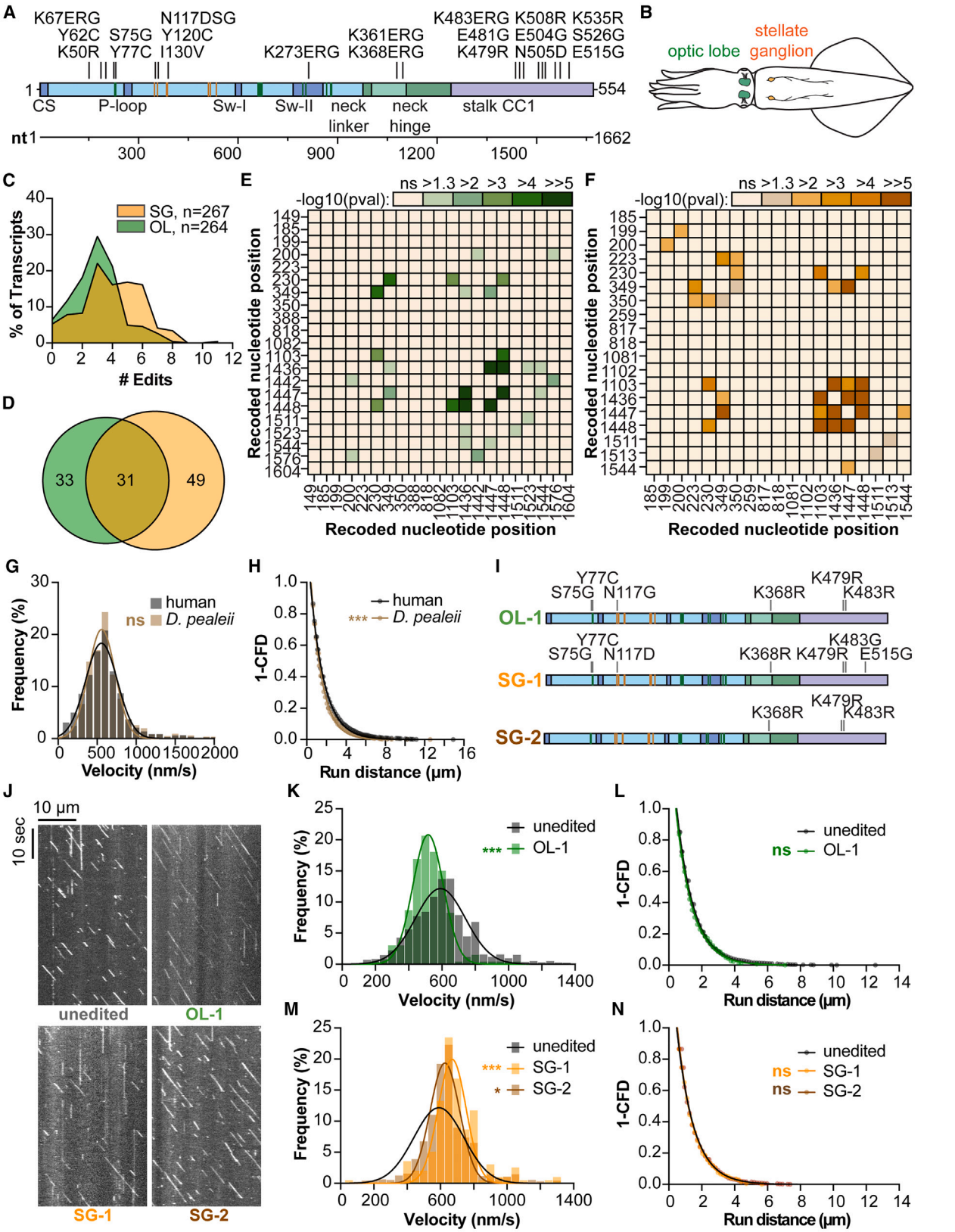

(legend on next page)

We next assessed the motile properties of different kinesin variants identified from the optic lobe and the stellate ganglion. We first generated an unedited GFP-tagged *D. pealeii* kinesin construct (*D. peal*K554), purified the recombinant protein, and quantified its motile properties in single-molecule motility assays. Unedited *D. pealeii* kinesin displayed similar velocities and modestly shorter run distances compared to human kinesin (*human* K560[18]) (Figures 2G and 2H). We then compared the motility of different recoded *D. pealeii* kinesin variants found in the optic lobe and stellate ganglion (Figure 2I) to unedited *D. pealeii* kinesin. Recoded variants displayed significantly different motility characteristics compared to unedited *D. pealeii* kinesin (Figures 2J–2N; Table S2). A variant unique to the optic lobe (OL-1) displayed decreased velocity (Figure 2K), while two variants unique to the stellate ganglion (SG-1 and SG-2) displayed increased velocity (Figure 2M). Together, these data indicate that RNA recoding in different tissues is capable of generating unique kinesin variants with distinct motile properties. The increased velocities we observed in stellate ganglion-specific kinesin variants may reflect a need for faster long-distance axonal transport in these cells.

Recoding of kinesin in wild squid is responsive to seawater temperature

Ocean temperature is a dynamic and ecologically relevant environmental factor for *Doryteuthis* squid. In the wild, these animals experience a broad range of temperatures during seasonal and daily depth migrations, frequenting waters as cold as 6°C.[19,20] The motility of human kinesins changes dramatically with temperature *in vitro*; for example, human KIF5B[21] and KIF5A[22,23] display decreased velocities and shorter run distances as temperature decreases. Unlike humans, cephalopods are ectotherms.[24,25] We therefore wondered if temperature-dependent RNA recoding of kinesin could be one mechanism squid employ to modulate kinesin motility in different ocean temperatures. We hypothesized that RNA recoding could provide a homeostatic mechanism to maintain transport functions as these animals experience fluctuations in ocean temperature.

We examined the effects of ocean temperature on recoding of the kinesin motor domain of the opalescent inshore squid *Doryteuthis opalescens*. These animals make seasonal spawning migrations along the coast of San Diego,[19] providing us local access to a squid population. We sequenced the *D. opalescens* kinesin motor domain from cDNA and found that it is 99.5% identical to *D. pealeii* (Figures S3A–S3C). To identify recoding sites in the *D. opalescens* kinesin motor domain, we compared our genomic sequence of the kinesin motor domain to 87 individual cDNA clones from the same individual animal (Figure S3D). We identified 14 recoding sites, all of which overlapped with sites previously identified from *D. pealeii*.

We first asked if RNA recoding of the *D. opalescens* kinesin motor domain changes in response to seawater temperature. *D. opalescens* egg casings were collected from the ocean, and hatchlings (Figure 3A) were transferred to temperature-controlled seawater tanks for 24 h before extracting RNA from individual whole animals (Figure 3B). We exposed animals to water temperatures ranging from 6°C to 20°C, which encompasses the extreme range of temperatures these animals experience in the wild.[19,20,26] We then sequenced kinesin from total cDNA to determine RNA editing levels at each individual recoding site along the kinesin motor domain from animals exposed to each temperature. For most of the detected recoding sites in the kinesin motor domain, percent editing significantly increased as temperature decreased (Figure 3C).

Figure 2. Tissue-specific recoding of squid kinesin generates functionally distinct motors

(A) Schematic indicating recoded amino acids along the squid *D. pealeii* kinesin-1 motor domain (amino acids 1–554). The motor head is in blue, the neck is in green, and the stalk is in purple. A nucleotide (nt) ruler is shown below. Only recoding sites detected in this study from clone sequencing of the stellate ganglion and optic lobe are depicted. See Table S3 for additional reported recoding sites in kinesin.

(B) Cartoon of *D. pealeii* with optic lobes and stellate ganglion indicated.

(C and D) Summary of clone sequencing of *D. pealeii* kinesin cDNA from the optic lobe (green) and stellate ganglion (orange). Percent of transcripts detected with multiple edit sites (C) and number of unique transcripts detected (D) for each tissue. See also Figure S2.

(E and F) Pairwise correlations between recoding sites along the *D. pealeii* kinesin motor domain from the optic lobe (E) and stellate ganglion (F). Color indicates $-\log_{10}$ (p value).

(G) Velocity analysis of human kinesin (gray) and unedited *D. pealeii* kinesin (brown). Histograms were fit to a Gaussian. The mean ± SD of the Gaussian fit for human kinesin is 554.9 ± 204.1 nm/s and for *D. pealeii* kinesin is 558.5 ± 172.2 nm/s.

(H) Run distance analysis of human kinesin (gray) and unedited *D. pealeii* kinesin (brown). 1-cumulative frequency distributions (1-CFD) were fit to a one-phase exponential decay. The 95% confidence interval (CI) of the mean decay constant (tau) for human kinesin is 1.374–1.447 μm and for *D. pealeii* kinesin is 1.116–1.175 μm.

(I) *D. pealeii* recoding site variants generated in *D. pealeii* kinesin. Variant OL-1 is specific to the optic lobe, and variants SG-1 and SG-2 are specific to the stellate ganglion.

(J) Representative kymographs of unedited *D. pealeii* kinesin and variants OL-1, SG-1, and SG-2.

(K) Velocity analysis of OL-1 (green) compared to unedited *D. pealeii* kinesin (gray). Mean ± SD for OL-1 is 520.6 ± 89.43 nm/s, for unedited is 587.1 ± 158.1 nm/s.

(L) Run distance analysis of OL-1 (green) compared to unedited *D. pealeii* kinesin (gray). The 95% CI of tau for OL-1 is 0.9792–1.053 μm, for unedited is 1.016–1.058 μm.

(M) Velocity analysis of SG-1 (orange) and SG-2 (brown) compared to unedited *D. pealeii* kinesin (black line shows fit from K). Mean ± SD for SG-1 is 674.3 ± 111.4 nm/s, for SG-2 is 620.6 ± 97.26 nm/s.

(N) Run distance analysis of SG-1 (orange) and SG-2 (brown) compared to unedited *D. pealeii* kinesin (black line shows fit from L). The 95% CI of tau for SG-1 is 0.9682–1.013 μm, for SG-2 is 0.9411–1.033 μm.

For all motility data, data were pooled from at least 2 independent protein preparations. Significance was calculated by two-tailed t test comparing the means for all velocity comparisons or comparing the rate constants for all run distance comparisons. See Table S2 for fit parameters and exact p values for all statistical tests. In all figures, stars indicate the following p values: ***, $p < 0.0001$; **, $p < 0.001$; *, $p < 0.01$; ns, $p > 0.01$.

See also Figure S1.

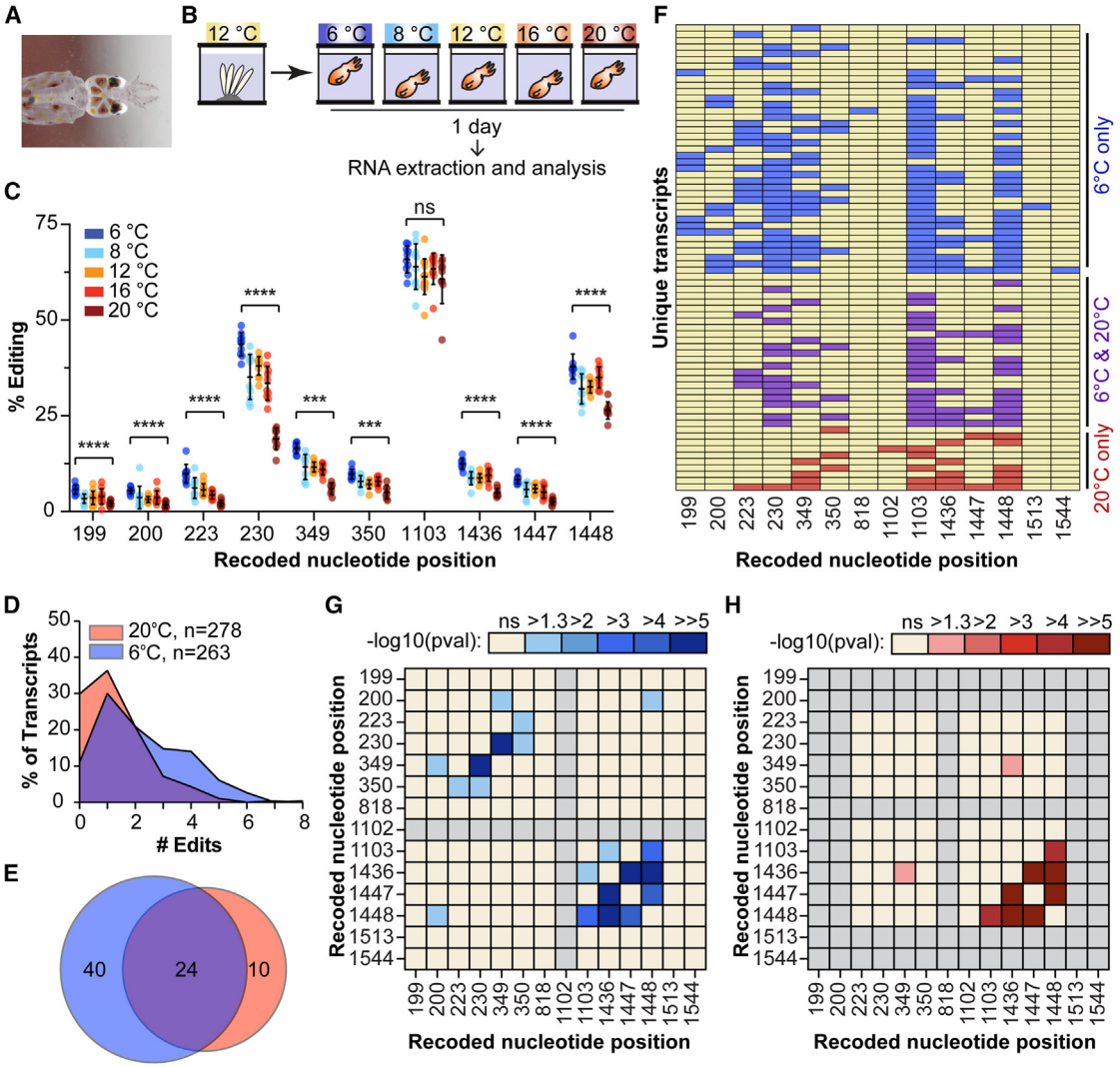

Figure 3. Squid kinesin transcripts are differentially recoded in response to seawater temperature

(A) Photograph of a *D. opalescens* hatchling.

(B) Schematic of temperature assay. *D. opalescens* egg casings were maintained at 12°C, and hatchlings were transferred to tanks maintained at specified seawater temperatures for 24 h, then animals were collected for RNA extraction and analysis.

(C) Percent editing at recoding sites along the *D. opalescens* kinesin-1 motor domain in individual animals exposed to different temperatures. Mean ± SD is shown, and significance was determined by Mann-Whitney test.

(D and E) Summary of clone sequencing of *D. opalescens* kinesin cDNA from animals exposed to either 6°C (blue) or 20°C (red) water. Percent of transcripts detected with multiple edit sites (D) and number of unique transcripts (E) for each temperature. See also Figures S4A and S4B.

(F) Unique recoding site combinations in *D. opalescens* kinesin from animals exposed to 6°C (blue) or 20°C (red) water or found in both (purple). Each row represents an individual clone sequence (transcript) and colored boxes indicate an A to G substitution at the nucleotide position (column) indicated.

(G and H) Pairwise correlations between recoding sites along the *D. opalescens* kinesin motor domain from animals exposed to 6°C (G) or 20°C (H) water. Color indicates -$\log_{10}$ (p value). Gray squares indicate recoding sites not detected.

See also Figure S3.

Next, we identified what kinesin recoding site combinations were generated in animals exposed to different seawater temperatures. We sequenced cDNA clones (representing individual kinesin transcripts) from animals exposed to either 6°C or 20°C seawater (Figures 3D–3F, S4A, and S4B). Consistent with our bulk sequencing results, we observed higher editing levels across kinesin transcripts from animals exposed to 6°C seawater as compared to 20°C seawater (Figure 3D). Sequencing individual transcripts allowed us to quantify the percentage of fully unedited transcripts; 30% of the transcripts sequenced from animals exposed to 20°C seawater were unedited, as compared to 11% unedited transcripts in animals exposed to 6°C seawater (Figure 3D). In addition, transcripts from animals exposed to 6°C were more extensively recoded,

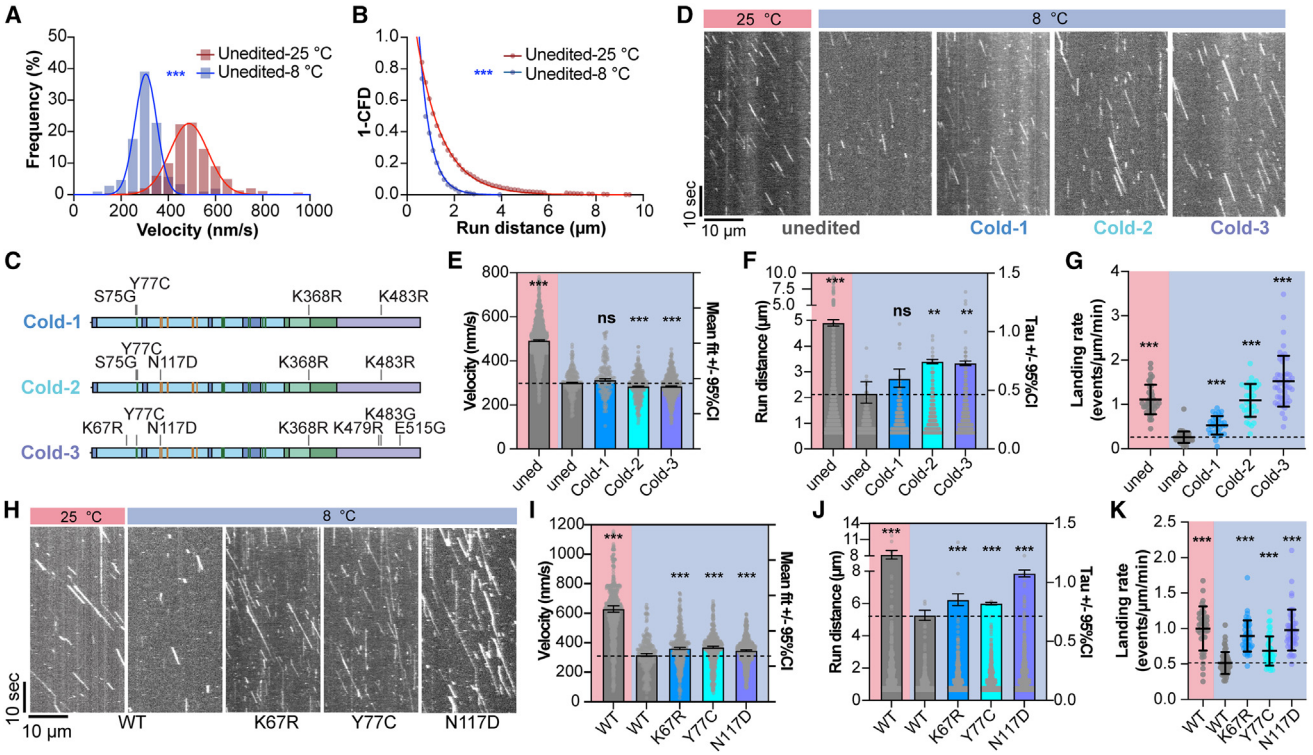

Figure 4. Cold-specific squid kinesin variants display enhanced motility in the cold

(A) Velocity analysis of unedited *D. opalescens* kinesin at 25°C (red) vs. 8°C (blue). Mean ± SD at 25°C is 487.4 ± 80.88 nm/s and at 8°C is 304.9 ± 46.29 nm/s.

(B) Run distance analysis of unedited *D. opalescens* kinesin at 8°C (blue) and 25°C (red). 95% CI of tau at 25°C is 1.049–1.103 μm and at 8°C is 0.3911–0.5728 μm.

(C) *D. opalescens* recoding site variants generated in *D. opalescens* kinesin: Cold-1, Cold-2, and Cold-3.

(D) Representative kymographs of unedited *D. opalescens* kinesin and variants Cold-1, Cold-2, and Cold-3.

(E) Velocity (nm/s) of Cold-1, Cold-2, and Cold-3 compared to unedited *D. opalescens* kinesin. Gray dots indicate individual measurements, and bars indicate 95% CI of the mean after fitting velocity histograms to a Gaussian. See also Figure S4C.

(F) Run distance (μm) of Cold-1, Cold-2, and Cold-3 compared to unedited *D. opalescens* kinesin. Gray dots indicate individual measurements (left Y axis), and bars (right Y axis) indicate 95% CI of tau after fitting 1-CFDs of run distance measurements to a one-phase decay. See also Figure S4D.

(G) Landing rates of Cold-1, Cold-2, and Cold-3 compared to unedited *D. opalescens* kinesin. Mean ± SD is indicated, and significance was calculated by two-tailed t test with Welch's correction.

(H) Representative kymographs of human kinesin substitutions K67R, Y77C, and N117D.

(I) Velocity (nm/s) of K67R, Y77C, and N117D compared to wild-type human kinesin. Gray dots indicate individual measurements, and bars indicate 95% CI of the mean. See also Figure S4J.

(J) Run distance analysis of K67R, Y77C, and N117D compared to wild-type human kinesin. Run distance (μm) of K67R, Y77C, and N117D compared to wild-type human kinesin. Gray dots indicate individual measurements (left Y axis), and bars (right Y axis) indicate 95% CI of tau. See also Figure S4K.

(K) Landing rates of K67R, Y77C, and N117D compared to wild-type human kinesin. Mean ± SD is indicated, and significance was calculated by two-tailed t test with Welch's correction.

See also Figure S1.

with 38% of transcripts harboring three or more recoding events as compared to 13% from animals exposed to 20°C (Figure 3D). Thus, RNA recoding of kinesin in *D. opalescens* squid is responsive to changes in ocean water temperature. Recoded variants of kinesin are preferentially generated in colder seawater, while unedited kinesin is preferred in warmer seawater. We also identified significant pairwise correlations between recoding sites, and some of these correlations were temperature specific (Figures 3G and 3H). This demonstrates that RNA recoding acutely generates temperature-specific kinesin variants in response to environmental temperature. In addition, our data indicate that temperature-dependent changes in RNA recoding can occur rapidly in animals, within 24 h.

Recoding enhances squid kinesin motility in the cold

We hypothesized that *D. opalescens* kinesin variants that were more extensively recoded in cold seawater might display enhanced motility *in vitro* at cold temperatures compared to unedited *D. opalescens* kinesin. We generated an unedited *D. opalescens* kinesin construct (*Dopal*K554) and measured its motile properties in single-molecule motility assays at 25°C and 8°C, which is the coldest temperature we could reliably cool our imaging set-up for single-molecule assays. Similar to human kinesin,[23] unedited *D. opalescens* kinesin exhibited slower velocities and shorter run distances in the cold (8°C) as compared to 25°C (Figures 4A and 4B). We generated three kinesin variants unique to animals exposed to cold seawater

(Figure 4C) and quantified the motile properties of these variants at 8°C and 25°C (Figures 4D–4G and S4C–S4H; Table S2). Two cold-specific *D. opalescens* kinesin variants (Cold-2 and Cold-3) displayed significantly longer run distances at 8°C compared to unedited *D. opalescens* kinesin, while slightly decreasing velocity (Figures 4E and 4F). In addition, all three cold-specific *D. opalescens* kinesin variants displayed significantly increased microtubule landing rates (the frequency of kinesin binding to the microtubule) at 8°C compared to unedited *D. opalescens* kinesin (Figure 4G). Thus, acute changes in RNA recoding of squid kinesin in response to cold ocean temperature generate kinesin variants with enhanced motile properties in the cold. This may be one mechanism squid use to optimize kinesin activity and intracellular transport of cargos in different environments (Figure 3H). The increase in mean landing rate we observed in cold-specific variants suggests a potential way in which these variants may be functionally enriched *in vivo* compared to unedited kinesin. For example, in cold temperatures, edited kinesin variants may be able to bind microtubule tracks more efficiently than unedited kinesin to promote transport.

Cold-preferred recoding site substitutions enhance human kinesin motility in the cold

Three amino acids changes (Lys67Arg, Tyr77Cys, and Asn117Asp) found in the cold-specific kinesin variants we tested occurred significantly more often across recoded squid kinesin transcripts from animals exposed to cold water than in animals exposed to warm water (Figures 3F and S4I). To determine what effect these cold-preferred substitutions would have individually on kinesin motility, we generated Lys67Arg, Tyr77Cys, and Asn117Asp substitutions in a truncated GFP-tagged human kinesin construct (K560[18]; here "human kinesin") and assessed motility at 8°C compared to wild-type human kinesin. (Figures 4I–4K, S4J, and S4K; Table S2). We found that each of these individual substitutions significantly increased run distance and landing rate of human kinesin at 8°C compared to wild-type human kinesin (Figure 6H). Given that these substitutions are enriched across cold-specific squid kinesin transcripts, it is possible that higher landing rates and increased run distance may be general features of kinesin variants generated in these animals after exposure to cold seawater.

Recoding sites occur in conserved amino acids across kinesin and dynein

Our results with squid kinesin support the idea that RNA recoding has the potential to dynamically modulate protein function in different tissues and environmental conditions. We found that recoding generates a diversity of complex variants containing different combinations of recoded amino acids. Considered individually, many recoding sites occur in conserved amino acids; for example, 24/31 (77%) of the recoded amino acids in the *D. pealeii* kinesin motor domain are conserved in human kinesin. Our data looking at cold-preferred squid substitutions in human kinesin support that individual cephalopod recoding site substitutions can alter protein function in non-cephalopod proteins. We therefore sought to characterize the effects of cephalopod recoding site substitutions in kinesin, as well as dynein, within well-studied homologs of these motors: human kinesin and yeast dynein.

We first surveyed reported cephalopod recoding sites across kinesin and dynein. We mined previously published editome data from six cephalopod species.[5–8] Dynein and kinesin are highly conserved between these cephalopod species and human, sharing ~74% and ~65% amino acid sequence identity, respectively. Both motors are extensively recoded across cephalopods, and recoding sites are widely distributed across conserved and non-conserved amino acids (Figures 5A and 5B; Tables S3 and S4). Across the six cephalopod species we analyzed, there are 154 total possible recoding events in kinesin, 55 of which are shared amongst multiple cephalopod species, and 500 total recoding events in dynein, 125 of which are shared.

Kinesin and dynein are both dimeric motors that use the energy from ATP hydrolysis to generate conformational changes that ultimately drive unidirectional movement along the microtubule.[27–29] Dynein's motor domain contains a ring of AAA+ domains, and the nucleotide state at AAA1 and AAA3 governs the affinity between dynein's microtubule binding domain (MTBD) and the microtubule. A long anti-parallel coiled-coil "stalk" and a shorter coiled-coil "buttress" connect dynein's AAA+ ring to the MTBD, while the "linker" connects dynein's AAA+ ring to the cargo binding end of the motor and makes large movements during dynein's ATP hydrolysis cycle that generate force.[30–32] Prior to activation, the dynein dimer exists in an autoinhibited "Phi" conformation that involves contacts between dynein's stalk, AAA+ domains, and linker.[33] Kinesin's motor domain is much smaller and more compact compared to dynein, with its single ATP binding and microtubule binding sites in close proximity.[34] The motor domain of kinesin is connected to its coiled-coil dimerization and cargo binding domains via the "neck-linker," which undergoes cycles of docking and undocking from the motor domain in a nucleotide-dependent manner.[35] Kinesin also has an autoinhibited state, where its tail domain interacts with the motor.[36,37]

Some recoding sites occur in conserved amino acids within known mechanical elements of kinesin and dynein, but the specific substitutions generated through recoding at these sites have not been explored (Figures 5C and 5D). For example in dynein, amino acid contact sites between the motor domain and the linker are recoded,[30–32] as are contact sites important for stabilizing the auto-inhibited Phi form of dynein.[33] In kinesin, amino acids involved in neck linker docking,[38,39] microtubule binding,[40] as well as tail peptide autoinhibition[36] are also recoded. To our knowledge, only two out of the combined 540 recoded amino acids across kinesin and dynein overlap with amino acids previously associated with disease,[41] and recoding substitutions differ from disease-associated mutations at these sites. The vast majority of recoding sites in both kinesin and dynein occur in amino acids that have not been previously highlighted as functionally important. Thus, cephalopod recoding sites point to residues and substitutions that are not readily predicted by other methods.

By focusing on amino acid residues in yeast dynein and human kinesin that are both conserved with and recoded in cephalopods, we dramatically reduce the number of substitutions to evaluate. For example, ~1,265 residues are conserved between

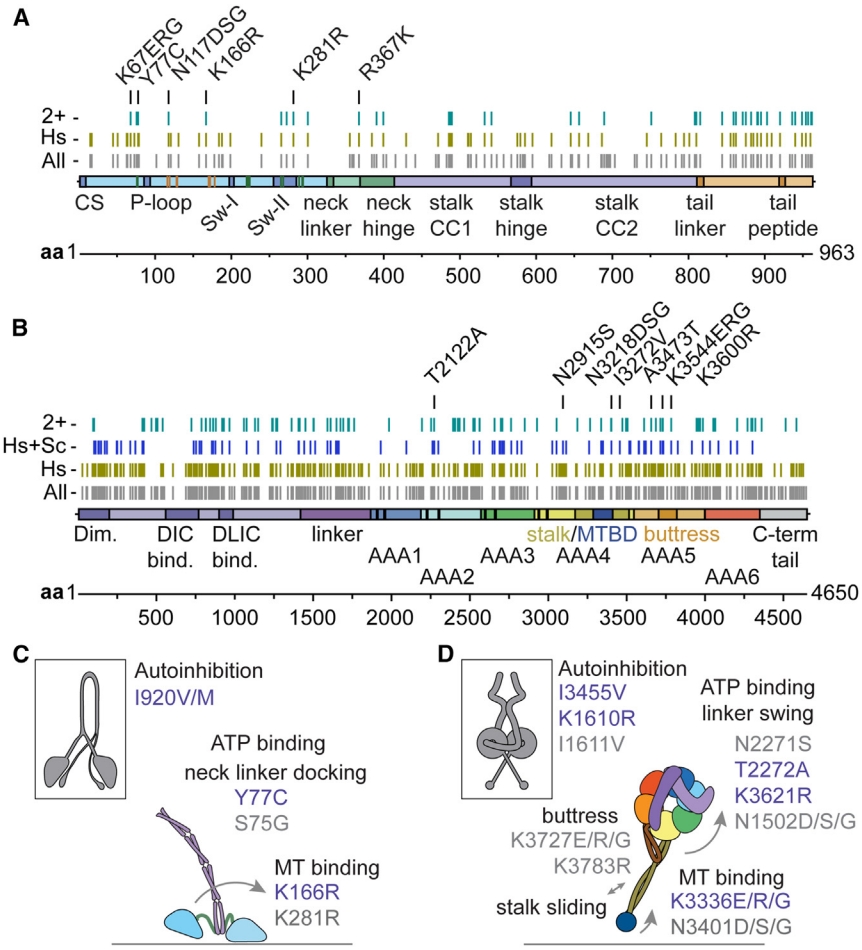

Figure 5. Cephalopod recoding sites occur in conserved residues in dynein and kinesin

(A and B) Cephalopod recoding sites distributed across the kinesin-1 heavy chain (A) and the cytoplasmic dynein-1 heavy chain-1 (B). Domain features are indicated. "All" indicates all reported recoded amino acid positions in cephalopods. "Hs" indicates amino acids that are recoded in at least one species of cephalopod and are also conserved with human KIF5B or human DYNC1H1; "Hs+Sc" indicates amino acids that are recoded in in at least one species of cephalopod and are also conserved with both human DYNC1H1 and *S. cerevisiae* Dyn1; "2+" indicates recoding sites that are shared across 2 or more cephalopod species. Amino acid substitutions we characterized in human K560 kinesin or yeast GST-Dyn1(331kDa) dynein are indicated. See Tables S3 and S4 for a list of reported recoding sites in kinesin and dynein, respectively.

(C and D) Schematics showing select cephalopod recoding sites associated with mechanochemical elements important for kinesin (C) and dynein (D) motility. Amino acids that have been previously implicated in each process are shown in blue, and sites that may be involved are shown in gray. Amino acid numbering is from human KIF5B and human DYNC1H1.

human, yeast, and cephalopod dynein, but only 89 of these residues are also recoded in any species of cephalopod. In addition, recoding guides what specific substitutions to evaluate. These substitutions represent natural variants found in cephalopods, and animals may employ either the recoded or the genome-encoded residue in different contexts. We assessed the effects of recoding site substitutions in well-characterized minimal motor constructs; for human kinesin, we used K560[18] ("human kinesin"), and for yeast dynein, we used a truncated, GST-dimerized construct[42] (GST-Dyn1(331kDa), "yeast dynein"). We focused on sites conserved within the motor domains of these minimal constructs that are recoded in at least 2% of RNAs from RNA-sequencing data[5–8] of any one cephalopod species. Applying these criteria, we generated a panel of 10 recoding site substitutions across six amino acids in human kinesin (Figure 5A) and 11 recoding site substitutions across seven amino acids in yeast dynein (Figure 5B).

For each substitution, we quantified velocity, run distance, and fraction of processive events in single-molecule motility assays (Figures 6, S5, and S6; Table S2). The majority of amino acid substitutions we assessed in both human kinesin and yeast dynein significantly altered motility. Unlike disease-associated mutations in kinesin and dynein,[43–45] none of the cephalopod-guided substitutions we made abolished processivity, and most significantly increased run distance or velocity. Most of the substitutions we analyzed occur in previously uncharacterized amino acids, indicating that cephalopod recoding sites can be used as a guide to identify conserved residues of functional importance. We highlight examples for both motors below. For discussion of additional substitutions characterized, refer to Figures S5 and S6.

Recoding site substitutions alter human kinesin motility

In kinesin, 27 amino acids in the motor head are recoded in at least one species of cephalopod, and 22 of these amino acids are conserved with human kinesin. We assessed recoding site substitutions in five of these amino acids: K67, Y77, N117, K166, and K281. Three of these residues (K67, Y77, and N117) were also characterized in our analysis of cold-specific recoding in *D. opalescens* (Figures 4H–4K).

Tyr77 is predicted to help stabilize formation of the cover neck bundle (CNB) and neck linker docking,[38] and an aromatic residue at this position is highly conserved across kinesins.[39] The analogous site in Kif1A (Tyr89) is mutated to Asp in hereditary spastic paraplegia (HSP), and in single molecule motility assays, Tyr89Asp results in slower velocities and increased run distance.[39] Tyr77 can be edited to a Cys in multiple cephalopod species. We found that a Tyr77Cys substitution in human kinesin resulted in increased run distance without significantly altering velocity (Figures 6B and 6C), which is consistent with a role for this residue in stabilizing neck linker docking.

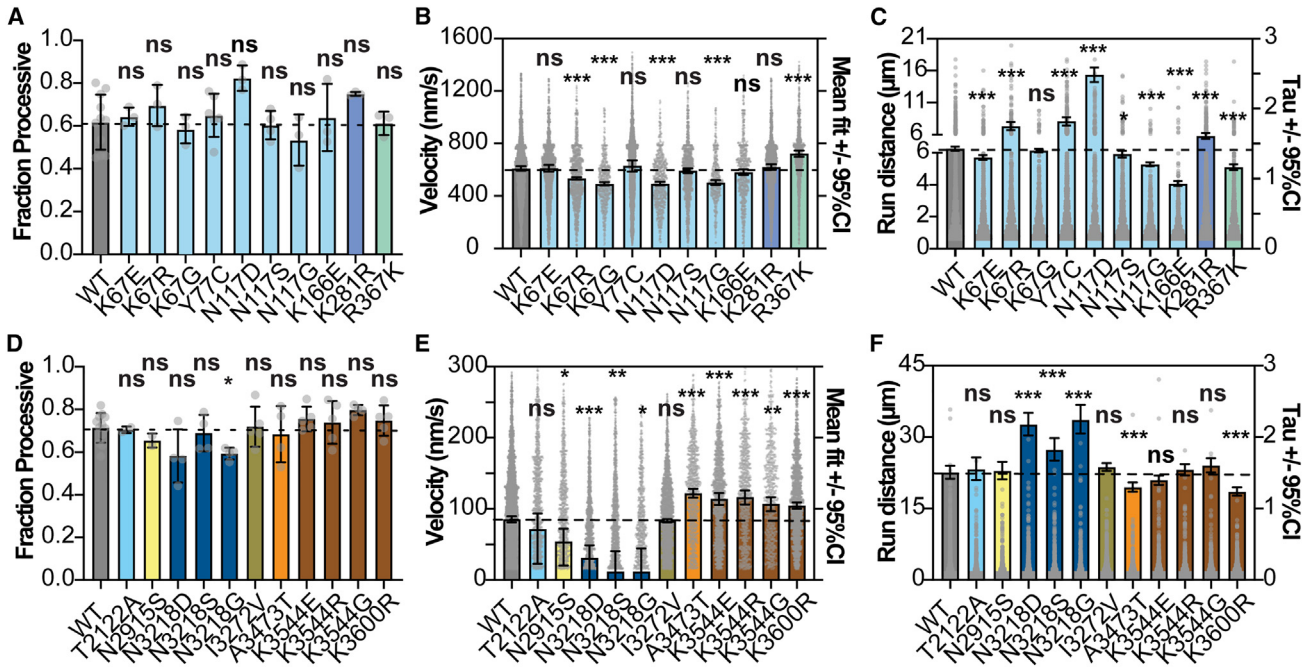

Figure 6. Recoding site substitutions tailor the motility of human kinesin and yeast dynein

(A) Fraction processive for each human kinesin mutant. Mean ± SD is indicated, and significance was calculated by two-tailed t test.

(B) Velocity (nm/s) of each human kinesin mutant. Gray dots indicate individual measurements, and bars indicate 95% CI of the mean.

(C) Run distance (μm) of each human kinesin mutant. Gray dots indicate individual measurements (left Y axis), and bars (right Y axis) indicate 95% CI of tau.

(D) Fraction processive for each yeast dynein mutant. Mean ± SD is indicated, and significance was calculated by two-tailed t test.

(E) Velocity (nm/s) of each yeast dynein mutant. Gray dots indicate individual measurements, and bars indicate 95% CI of the mean.

(F) Run distance (μm) of each yeast dynein mutant. Gray dots indicate individual measurements (left Y axis), and bars (right Y axis) indicate 95% CI of tau.

See Figures S5 and S6 for frequency distributions and representative kymographs for each human kinesin mutant and yeast dynein mutant respectively.

See also Figure S1.

Both Asn117 and Lys67 are surface-exposed residues for which there is little functional insight. Asn117 can be edited to Asp, Ser, or Gly, and a recent structure of kinesin bound to microtubules suggests that Asn117 is involved in neck linker docking.[46] We found that Asn117Asp markedly increased run distance and decreased velocity, while Asn117Ser had little effect on run distance or velocity, and Asn117Gly decreased both velocity and run distance (Figures 6B and 6C). Lys67 can be edited to Glu, Arg, or Gly. We found that Lys67Glu resulted in a modest decrease in run distance, while Lys67Arg increased run distance and decreased velocity (Figures 6B and 6C). These effects suggest that Lys67 may be involved in stabilizing long-range electrostatic interactions with the microtubule, similar to the computationally predicted role for the adjacent residue Lys68.[47]

We also evaluated the effects of recoding site substitutions in Lys166 and Lys281, which are both located along the microtubule interaction face of the motor domain. Mutation of these residues to alanine results in decreased microtubule binding.[40] Lys281Ala has been shown to display a more severe effect on microtubule binding compared to Lys166Ala, and mutation of an adjacent residue (Arg280) to serine in KIF5A, which is mutated in HSP,[48,49] also results in decreased microtubule binding affinity.[50,51] In *O. bimaculoides* and *O. vulgaris*, Lys281 is recoded to Arg, which would be expected to strengthen the electrostatic interaction between the motor head and the microtubule. In *S. officinalis*, Lys166 can be recoded to Glu, which would be expected to weaken the interaction with the microtubule. We found that Lys281Arg modestly increased run distance, while Lys166Glu decreased run distance (Figures 6B and 6C), which is consistent with the proposed role for these residues in stabilizing electrostatic interactions with the microtubule.

Recoding site substitutions alter yeast dynein motility

Next, we evaluated the effects of recoding site substitutions on dynein motility. In dynein, several recoding site substitutions occur in the buttress. Deletion of the buttress/stalk interaction loop decouples ATPase activity from microtubule binding[30] and abolishes motility,[52] but there is limited insight into specific buttress residues outside of the buttress/stalk interaction loop. Ten amino acids within the buttress are sites of cephalopod recoding, and five of these are conserved with yeast dynein. We characterized recoding site substitutions in two of these amino acids located along the buttress coiled coil: Lys3544, located in coiled-coil 1 (CC1), and Lys3600, located in CC2. Lys3544 can be recoded to Glu, Arg, or Gly, and we found that substitution to any of these diverse amino acids increased velocity of yeast dynein without markedly altering run distance (Figures 6E and 6F). Lys3600 is recoded to Arg, and

Lys3600Arg resulted in increased velocity and decreased run distance compared to wild-type dynein (Figures 6E and 6F). The effects of these substitutions highlight unexplored residues in the buttress that significantly influence motility.

We also characterized recoding site substitutions in the microtubule binding domain (MTBD) of dynein. Eight amino acids in the MTBD are recoded in cephalopods, and four of these amino acids are conserved with yeast dynein. We assessed the effects of recoding site substitutions in Asn3218, which is located in CC2 of the stalk as it exits the MTBD[53,54] and is not predicted to directly contact the microtubule. Asn3218 can be recoded to Asp, Ser, or Gly, and we found that each of these substitutions in yeast dynein resulted in decreased velocity and increased run distance compared to wild type. (Figures 6E and 6F). Although Asn3218 is not predicted to directly interact with the microtubule lattice, it is possible this amino acid interacts with the long unstructured C-terminal tails of tubulin and that mutations to Asp, Ser, or Gly increase these interactions given the phenotypes we observe.

This survey of recoding site substitutions in human kinesin and yeast dynein illustrates how cephalopod recoding sites can reveal conserved amino acids with subtle effects on protein function and further highlights a role for RNA recoding in diversifying protein function.

DISCUSSION

Our results support that cephalopods use RNA recoding as a mechanism for generating phenotypic plasticity. We show that squid can flexibly tune kinesin function through RNA recoding in different tissues and environmental temperatures which may support physiological needs and acclimation to changing environmental conditions. These data provide evidence supporting the long-standing hypothesis that RNA recoding may be involved in temperature acclimation.[11,17,55] Organisms employ diverse molecular mechanisms to compensate for environmental temperature variation[56,57] and temperature-dependent recoding of kinesin or other proteins may be an important component of temperature acclimation in other animals as well, such as *Drosophila* and hibernating mammals, where global temperature-dependent changes in RNA editing have been described.[58–61]

Our analysis of squid kinesin transcripts motivates future work exploring the mechanisms regulating combinatorial RNA editing. Edit sites are typically determined from short-read RNA sequencing, and thus for most transcripts, it is unknown how edit sites occur in combination along the same transcript. In humans, combinatorial editing of the serotonin 2C receptor can generate functionally distinct receptor variants, and dysregulated editing has been correlated with neurological disorders.[62–66] We identified tissue-specific and temperature-specific recoding site combinations in squid kinesin, which encoded variants with distinct motile properties. Similar to previous studies, we detected significant correlations between edit sites.[67] Our work also suggests that correlations in recoding between sites can be condition specific, suggestive of condition-specific regulation of combinatorial editing. Such regulation could be mediated at the level of ADAR expression or localization, differential RNA localization or folding, or through interaction with other RNA binding proteins. Indeed, tissue-specific differences in combinatorial editing of the Shaker potassium channel in *Drosophila* appear to involve regulation beyond differences in ADAR expression level alone.[68] For recoding of squid kinesin, it is unknown which ADARs are responsible for editing at which sites, or where (nucleus vs. cytoplasm) recoding may be occurring. For example, unlike mammalian ADAR2, squid ADAR2 has been shown to localize to both the nucleus and cytoplasm,[16] opening up additional modes of potential regulation. Emerging long-read RNA sequencing methods[69,70] should offer an opportunity in the future to widely assess combinatorial RNA editing across diverse cell-types, subcellular compartments, and conditions.

Our survey of recoding site substitutions in human kinesin and yeast dynein highlights how the cephalopod editome can be used to interrogate the function of conserved proteins. Multiple protein sequence alignments provide a comparative genetic approach to infer regions of conserved function. Cephalopod RNA editing offers an epigenetic lens to further pinpoint functionally important substitutions in conserved residues, complementing insights gained by homology alone. This approach may be especially useful in protein regions where *a priori* identification of amino acid residues important for function is challenging and could be used to identify amino acid substitutions that enhance or tailor protein function under different contexts. Thus, we propose that cephalopod recoding sites represent a general resource and guide for characterizing other proteins. For example, numerous disease-associated proteins are highly recoded in cephalopods (eg. Tau, Amyloid beta, LRRK2), and characterizing recoding sites may offer a fresh perspective into the regulation and function of these proteins.

Limitations of the study

This study evaluated the effects of recoding on single-molecule motility of minimal motor constructs, but our survey of edit sites in dynein and kinesin suggests that recoding also likely affects other motor protein characteristics such as ATPase activity, microtubule binding, force generation, and auto-inhibition mechanisms. In addition, it will be interesting to explore how recoding affects other processes such as protein turnover, cargo binding, complex assembly, and trafficking. Our data indicate that temperature-dependent changes in editing can occur rapidly in animals (<24 h), but it is unclear how quickly edited transcripts are translated and transport components are turned over; future proteomic studies may help clarify this. *In vivo*, we imagine that a mixture of kinesin-1 variants becomes biased toward highly recoded variants when animals are exposed to cold temperatures. Characterizing the motility of mixed motor populations in gliding assays as well as single-molecule motility of heterodimers could help delineate the effects of this heterogeneity. Our data suggest that landing rate and run distance are important motility parameters modulated by RNA recoding of kinesin in response to cold temperature, and this provides a possible mechanism for the functional enrichment of recoded kinesin variants *in vivo*. However, future work assessing the effects of recoding on other aspects of motility is warranted. Microtubule-based transport involves hundreds of proteins, and it will be interesting to evaluate

how recoding is coordinated across various components of the transport machinery *in vivo*, especially in the context of temperature acclimation.

STAR★METHODS

Detailed methods are provided in the online version of this paper and include the following:

- KEY RESOURCES TABLE
- RESOURCE AVAILABILITY
  - Lead contact
  - Materials availability
  - Data and code availability
- EXPERIMENTAL MODEL AND SUBJECT DETAILS
  - Animals
  - Yeast strains
- METHOD DETAILS
  - Mapping of edit sites
  - Gene ontology (GO) term enrichment analysis
  - Identification of recoding sites in the kinesin motor domain of *D. opalescens*
  - Strain generation
  - Protein purification
  - TIRF microscopy
  - Motility assays
  - Kymograph analysis
  - Determination of edit site combinations from *D. pealeii* tissues
  - *D. opalescens* temperature experiment
  - Determination of editing levels and edit site combinations in *D. opalescens*
- QUANTIFICATION AND STATISTICAL ANALYSIS
  - Statistical analysis of motility assays
  - Statistical analysis of combinatorial editing
  - Statistical analysis of editing levels per site between 6°C and 20°C

SUPPLEMENTAL INFORMATION

Supplemental information can be found online at https://doi.org/10.1016/j.cell.2023.04.032.

ACKNOWLEDGMENTS

We wish to thank Aaditya Rangan at the Courant Institute of Mathematical Sciences at NYU for pairwise correlation analysis of combinatorial RNA editing, Donovan Ventimiglia for help designing and coding the kymograph analysis software, Phil Zerofski at the Scripps Institute for Oceanography at UC San Diego for collecting *D. opalescens* egg cases, Lilly McCormick for help setting up tanks, Joshua Rosenthal at the Marine Biological Laboratory for gifting *D. pealeii* tissue samples. We thank Andres Leschziner, Donovan Ventimiglia, and members of the Reck-Peterson lab for feedback on the manuscript. K.J.R. is a Howard Hughes Medical Institute Awardee of the Life Sciences Research Foundation, and S.L.R.-P. is funded by the Howard Hughes Medical Institute and the National Institutes of Health grant R35 GM141825.

AUTHOR CONTRIBUTIONS

K.J.R. and S.L.R.-P. conceived of the study. K.J.R. performed the experiments. K.J.R. and S.L.R.-P. wrote the manuscript.

DECLARATION OF INTERESTS

The authors declare that they have no competing interests.

INCLUSION AND DIVERSITY

We support inclusive, diverse, and equitable conduct of research.

Received: October 10, 2022
Revised: March 5, 2023
Accepted: April 24, 2023
Published: June 8, 2023

REFERENCES

1. Nishikura, K. (2016). A-to-I editing of coding and non-coding RNAs by ADARs. Nat. Rev. Mol. Cell Biol. *17*, 83–96. https://doi.org/10.1038/nrm.2015.4.
2. Gabay, O., Shoshan, Y., Kopel, E., Ben-Zvi, U., Mann, T.D., Bressler, N., Cohen-Fultheim, R., Schaffer, A.A., Roth, S.H., Tzur, Z., et al. (2022). Landscape of adenosine-to-inosine RNA recoding across human tissues. Nat. Commun. *13*, 1184. https://doi.org/10.1038/s41467-022-28841-4.
3. Eisenberg, E. (2021). Proteome Diversification by RNA Editing. Methods Mol. Biol. *2181*, 229–251. https://doi.org/10.1007/978-1-0716-0787-9_14.
4. Rosenthal, J.J.C., and Eisenberg, E. (2023). Extensive Recoding of the Neural Proteome in Cephalopods by RNA Editing. Annu. Rev. Anim. Biosci. *11*, 57–75. https://doi.org/10.1146/annurev-animal-060322-114534.
5. Liscovitch-Brauer, N., Alon, S., Porath, H.T., Elstein, B., Unger, R., Ziv, T., Admon, A., Levanon, E.Y., Rosenthal, J.J.C., and Eisenberg, E. (2017). Trade-off between Transcriptome Plasticity and Genome Evolution in Cephalopods. Cell *169*, 191–202.e11. https://doi.org/10.1016/j.cell.2017.03.025.
6. Alon, S., Garrett, S.C., Levanon, E.Y., Olson, S., Graveley, B.R., Rosenthal, J.J.C., and Eisenberg, E. (2015). The majority of transcripts in the squid nervous system are extensively recoded by A-to-I RNA editing. Elife *4*, e05198. https://doi.org/10.7554/eLife.05198.
7. Shoshan, Y., Liscovitch-Brauer, N., Rosenthal, J.J.C., and Eisenberg, E. (2021). Adaptive Proteome Diversification by Nonsynonymous A-to-I RNA Editing in Coleoid Cephalopods. Mol. Biol. Evol. *38*, 3775–3788. https://doi.org/10.1093/molbev/msab154.
8. Albertin, C.B., Medina-Ruiz, S., Mitros, T., Schmidbaur, H., Sanchez, G., Wang, Z.Y., Grimwood, J., Rosenthal, J.J.C., Ragsdale, C.W., Simakov, O., and Rokhsar, D.S. (2022). Genome and transcriptome mechanisms driving cephalopod evolution. Nat. Commun. *13*, 2427. https://doi.org/10.1038/s41467-022-29748-w.
9. Moldovan, M., Chervontseva, Z., Bazykin, G., and Gelfand, M.S. (2020). Adaptive evolution at mRNA editing sites in soft-bodied cephalopods. PeerJ *8*, e10456. https://doi.org/10.7717/peerj.10456.
10. Jiang, D., and Zhang, J. (2019). The preponderance of nonsynonymous A-to-I RNA editing in coleoids is nonadaptive. Nat. Commun. *10*, 5411. https://doi.org/10.1038/s41467-019-13275-2.
11. Garrett, S., and Rosenthal, J.J.C. (2012). RNA editing underlies temperature adaptation in K+ channels from polar octopuses. Science *335*, 848–851. https://doi.org/10.1126/science.1212795.
12. Colina, C., Palavicini, J.P., Srikumar, D., Holmgren, M., and Rosenthal, J.J.C. (2010). Regulation of Na+/K+ ATPase transport velocity by RNA editing. PLoS Biol. *8*, e1000540. https://doi.org/10.1371/journal.pbio.1000540.
13. Rosenthal, J.J.C., and Bezanilla, F. (2002). Extensive editing of mRNAs for the squid delayed rectifier K+ channel regulates subunit tetramerization. Neuron *34*, 743–757. https://doi.org/10.1016/s0896-6273(02)00701-8.
14. Patton, D.E., Silva, T., and Bezanilla, F. (1997). RNA editing generates a diverse array of transcripts encoding squid Kv2 K+ channels with altered

functional properties. Neuron *19*, 711–722. https://doi.org/10.1016/s0896-6273(00)80383-9.

15. Holmgren, M., and Rosenthal, J.J.C. (2015). Regulation of Ion Channel and Transporter Function Through RNA Editing. Curr. Issues Mol. Biol. *17*, 23–36. https://doi.org/10.21775/cimb.017.023.
16. Vallecillo-Viejo, I.C., Liscovitch-Brauer, N., Diaz Quiroz, J.F., Montiel-Gonzalez, M.F., Nemes, S.E., Rangan, K.J., Levinson, S.R., Eisenberg, E., and Rosenthal, J.J.C. (2020). Spatially regulated editing of genetic information within a neuron. Nucleic Acids Res. *48*, 3999–4012. https://doi.org/10.1093/nar/gkaa172.
17. Rosenthal, J.J.C. (2015). The emerging role of RNA editing in plasticity. J. Exp. Biol. *218*, 1812–1821. https://doi.org/10.1242/jeb.119065.
18. Vale, R.D., Funatsu, T., Pierce, D.W., Romberg, L., Harada, Y., and Yanagida, T. (1996). Direct observation of single kinesin molecules moving along microtubules. Nature *380*, 451–453. https://doi.org/10.1038/380451a0.
19. Zeidberg, L. (2013). Doryteuthis opalescens, Opalescent Inshore Squid. In Advances in Squid Biology, Ecology and Fisheries. Part I – Myopsid Squids, R. Rosa, R. O'Dor, and G. Pierce, eds. (Nova Science Publishers Inc.), pp. 159–204.
20. Jacobson, L.D. (2005). Essential fish habitat source document. Longfin inshore squid, Loligo pealeii, life history and habitat characteristics. In NOAA Technical Memorandum NMFS-NE, *193*.
21. Kawaguchi, K., and Ishiwata, S. (2000). Temperature dependence of force, velocity, and processivity of single kinesin molecules. Biochem. Biophys. Res. Commun. *272*, 895–899. https://doi.org/10.1006/bbrc.2000.2856.
22. Doval, F., Chiba, K., McKenney, R.J., Ori-McKenney, K.M., and Vershinin, M.D. (2020). Temperature-dependent activity of kinesins is regulable. Biochem. Biophys. Res. Commun. *528*, 528–530. https://doi.org/10.1016/j.bbrc.2020.05.157.
23. Hong, W., Takshak, A., Osunbayo, O., Kunwar, A., and Vershinin, M. (2016). The Effect of Temperature on Microtubule-Based Transport by Cytoplasmic Dynein and Kinesin-1 Motors. Biophys. J. *111*, 1287–1294. https://doi.org/10.1016/j.bpj.2016.08.006.
24. Schickele, A., Francour, P., and Raybaud, V. (2021). European cephalopods distribution under climate-change scenarios. Sci. Rep. *11*, 3930. https://doi.org/10.1038/s41598-021-83457-w.
25. Burford, B.P., Wild, L.A., Schwarz, R., Chenoweth, E.M., Sreenivasan, A., Elahi, R., Carey, N., Hoving, H.-J.T., Straley, J.M., and Denny, M.W. (2022). Rapid Range Expansion of a Marine Ectotherm Reveals the Demographic and Ecological Consequences of Short-Term Variability in Seawater Temperature and Dissolved Oxygen. Am. Nat. *199*, 523–550. https://doi.org/10.1086/718575.
26. Zeidberg, L.D., Isaac, G., Widmer, C.L., Neumeister, H., and Gilly, W.F. (2011). Egg capsule hatch rate and incubation duration of the California market squid, Doryteuthis (Loligo) opalescens: insights from laboratory manipulations. Mar. Ecol. *32*, 468–479. https://doi.org/10.1111/j.1439-0485.2011.00445.x.
27. Carter, A.P., Diamant, A.G., and Urnavicius, L. (2016). How dynein and dynactin transport cargos: a structural perspective. Curr. Opin. Struct. Biol. *37*, 62–70. https://doi.org/10.1016/j.sbi.2015.12.003.
28. Bhabha, G., Johnson, G.T., Schroeder, C.M., and Vale, R.D. (2016). How Dynein Moves Along Microtubules. Trends Biochem. Sci. *41*, 94–105. https://doi.org/10.1016/j.tibs.2015.11.004.
29. Hancock, W.O. (2016). The Kinesin-1 Chemomechanical Cycle: Stepping Toward a Consensus. Biophys. J. *110*, 1216–1225. https://doi.org/10.1016/j.bpj.2016.02.025.
30. Kon, T., Oyama, T., Shimo-Kon, R., Imamula, K., Shima, T., Sutoh, K., and Kurisu, G. (2012). The 2.8 Å crystal structure of the dynein motor domain. Nature *484*, 345–350. https://doi.org/10.1038/nature10955.
31. Schmidt, H., Gleave, E.S., and Carter, A.P. (2012). Insights into dynein motor domain function from a 3.3-Å crystal structure. Nat. Struct. Mol. Biol. *19*, 492–497. https://doi.org/10.1038/nsmb.2272.
32. Roberts, A.J., Malkova, B., Walker, M.L., Sakakibara, H., Numata, N., Kon, T., Ohkura, R., Edwards, T.A., Knight, P.J., Sutoh, K., et al. (2012). ATP-Driven Remodeling of the Linker Domain in the Dynein Motor. Structure *20*, 1670–1680. https://doi.org/10.1016/j.str.2012.07.003.
33. Zhang, K., Foster, H.E., Rondelet, A., Lacey, S.E., Bahi-Buisson, N., Bird, A.W., and Carter, A.P. (2017). Cryo-EM Reveals How Human Cytoplasmic Dynein Is Auto-inhibited and Activated. Cell *169*, 1303–1314.e18. https://doi.org/10.1016/j.cell.2017.05.025.
34. Kull, F.J., Sablin, E.P., Lau, R., Fletterick, R.J., and Vale, R.D. (1996). Crystal structure of the kinesin motor domain reveals a structural similarity to myosin. Nature *380*, 550–555. https://doi.org/10.1038/380550a0.
35. Rice, S., Lin, A.W., Safer, D., Hart, C.L., Naber, N., Carragher, B.O., Cain, S.M., Pechatnikova, E., Wilson-Kubalek, E.M., Whittaker, M., et al. (1999). A structural change in the kinesin motor protein that drives motility. Nature *402*, 778–784. https://doi.org/10.1038/45483.
36. Kaan, H.Y.K., Hackney, D.D., and Kozielski, F. (2011). The structure of the kinesin-1 motor-tail complex reveals the mechanism of autoinhibition. Science *333*, 883–885. https://doi.org/10.1126/science.1204824.
37. Dietrich, K.A., Sindelar, C.V., Brewer, P.D., Downing, K.H., Cremo, C.R., and Rice, S.E. (2008). The kinesin-1 motor protein is regulated by a direct interaction of its head and tail. Proc. Natl. Acad. Sci. USA *105*, 8938–8943. https://doi.org/10.1073/pnas.0803575105.
38. Hwang, W., Lang, M.J., and Karplus, M. (2008). Force Generation in Kinesin Hinges on Cover-Neck Bundle Formation. Structure *16*, 62–71. https://doi.org/10.1016/j.str.2007.11.008.
39. Budaitis, B.G., Jariwala, S., Rao, L., Yue, Y., Sept, D., Verhey, K.J., and Gennerich, A. (2021). Pathogenic mutations in the kinesin-3 motor KIF1A diminish force generation and movement through allosteric mechanisms. J. Cell Biol. *220*, e202004227. https://doi.org/10.1083/jcb.202004227.
40. Woehlke, G., Ruby, A.K., Hart, C.L., Ly, B., Hom-Booher, N., and Vale, R.D. (1997). Microtubule Interaction Site of the Kinesin Motor. Cell *90*, 207–216. https://doi.org/10.1016/S0092-8674(00)80329-3.
41. Poirier, K., Lebrun, N., Broix, L., Tian, G., Saillour, Y., Boscheron, C., Parrini, E., Valence, S., Pierre, B.S., Oger, M., et al. (2013). Mutations in TUBG1, DYNC1H1, KIF5C and KIF2A cause malformations of cortical development and microcephaly. Nat. Genet. *45*, 639–647. https://doi.org/10.1038/ng.2613.
42. Reck-Peterson, S.L., Yildiz, A., Carter, A.P., Gennerich, A., Zhang, N., and Vale, R.D. (2006). Single-Molecule Analysis of Dynein Processivity and Stepping Behavior. Cell *126*, 335–348. https://doi.org/10.1016/j.cell.2006.05.046.
43. Hoang, H.T., Schlager, M.A., Carter, A.P., and Bullock, S.L. (2017). DYNC1H1 mutations associated with neurological diseases compromise processivity of dynein–dynactin–cargo adaptor complexes. Proc. Natl. Acad. Sci. USA *114*, E1597–E1606. https://doi.org/10.1073/pnas.1620141114.
44. Marzo, M.G., Griswold, J.M., Ruff, K.M., Buchmeier, R.E., Fees, C.P., and Markus, S.M. (2019). Molecular basis for dyneinopathies reveals insight into dynein regulation and dysfunction. Elife *8*, e47246. https://doi.org/10.7554/eLife.47246.
45. Jennings, S., Chenevert, M., Liu, L., Mottamal, M., Wojcik, E.J., and Huckaba, T.M. (2017). Characterization of kinesin switch I mutations that cause hereditary spastic paraplegia. PLoS One *12*, e0180353. https://doi.org/10.1371/journal.pone.0180353.
46. Zhang, C., Guo, C., Russell, R.W., Quinn, C.M., Li, M., Williams, J.C., Gronenborn, A.M., and Polenova, T. (2022). Magic-angle-spinning NMR structure of the kinesin-1 motor domain assembled with microtubules reveals the elusive neck linker orientation. Nat. Commun. *13*, 6795. https://doi.org/10.1038/s41467-022-34026-w.
47. Grant, B.J., Gheorghe, D.M., Zheng, W., Alonso, M., Huber, G., Dlugosz, M., McCammon, J.A., and Cross, R.A. (2011). Electrostatically Biased Binding of Kinesin to Microtubules. PLoS Biol. *9*, e1001207. https://doi.org/10.1371/journal.pbio.1001207.

48. Goizet, C., Boukhris, A., Mundwiller, E., Tallaksen, C., Forlani, S., Toutain, A., Carriere, N., Paquis, V., Depienne, C., Durr, A., et al. (2009). Complicated forms of autosomal dominant hereditary spastic paraplegia are frequent in SPG10. Hum. Mutat. *30*, E376–E385. https://doi.org/10.1002/humu.20920.

49. Fichera, M., Lo Giudice, M., Falco, M., Sturnio, M., Amata, S., Calabrese, O., Bigoni, S., Calzolari, E., and Neri, M. (2004). Evidence of kinesin heavy chain (KIF5A) involvement in pure hereditary spastic paraplegia. Neurology *63*, 1108–1110. https://doi.org/10.1212/01.wnl.0000138731.60693.d2.

50. Dutta, M., Diehl, M.R., Onuchic, J.N., and Jana, B. (2018). Structural consequences of hereditary spastic paraplegia disease-related mutations in kinesin. Proc. Natl. Acad. Sci. USA *115*, E10822–E10829. https://doi.org/10.1073/pnas.1810622115.

51. Ebbing, B., Mann, K., Starosta, A., Jaud, J., Schöls, L., Schüle, R., and Woehlke, G. (2008). Effect of spastic paraplegia mutations in KIF5A kinesin on transport activity. Hum. Mol. Genet. *17*, 1245–1252. https://doi.org/10.1093/hmg/ddn014.

52. Rao, L., Berger, F., Nicholas, M.P., and Gennerich, A. (2019). Molecular mechanism of cytoplasmic dynein tension sensing. Nat. Commun. *10*, 3332. https://doi.org/10.1038/s41467-019-11231-8.

53. Redwine, W.B., Hernandez-Lopez, R., Zou, S., Huang, J., Reck-Peterson, S.L., and Leschziner, A.E. (2012). Structural basis for microtubule binding and release by dynein. Science *337*, 1532–1536. https://doi.org/10.1126/science.1224151.

54. Lacey, S.E., He, S., Scheres, S.H., and Carter, A.P. (2019). Cryo-EM of dynein microtubule-binding domains shows how an axonemal dynein distorts the microtubule. Elife *8*, e47145. https://doi.org/10.7554/eLife.47145.

55. Yablonovitch, A.L., Deng, P., Jacobson, D., and Li, J.B. (2017). The evolution and adaptation of A-to-I RNA editing. PLoS Genet. *13*, e1007064. https://doi.org/10.1371/journal.pgen.1007064.

56. Somero, G.N. (2022). The Goldilocks Principle: A Unifying Perspective on Biochemical Adaptation to Abiotic Stressors in the Sea. Ann. Rev. Mar. Sci *14*, 1–23. https://doi.org/10.1146/annurev-marine-022521-102228.

57. Clark, M.S., and Worland, M.R. (2008). How insects survive the cold: molecular mechanisms—a review. J. Comp. Physiol. B *178*, 917–933. https://doi.org/10.1007/s00360-008-0286-4.

58. Rieder, L.E., Savva, Y.A., Reyna, M.A., Chang, Y.-J., Dorsky, J.S., Rezaei, A., and Reenan, R.A. (2015). Dynamic response of RNA editing to temperature in Drosophila. BMC Biol. *13*, 1. https://doi.org/10.1186/s12915-014-0111-3.

59. Buchumenski, I., Bartok, O., Ashwal-Fluss, R., Pandey, V., Porath, H.T., Levanon, E.Y., and Kadener, S. (2017). Dynamic hyper-editing underlies temperature adaptation in Drosophila. PLoS Genet. *13*, e1006931. https://doi.org/10.1371/journal.pgen.1006931.

60. Riemondy, K.A., Gillen, A.E., White, E.A., Bogren, L.K., Hesselberth, J.R., and Martin, S.L. (2018). Dynamic temperature-sensitive A-to-I RNA editing in the brain of a heterothermic mammal during hibernation. RNA *24*, 1481–1495. https://doi.org/10.1261/rna.066522.118.

61. Duan, Y., Dou, S., Luo, S., Zhang, H., and Lu, J. (2017). Adaptation of A-to-I RNA editing in Drosophila. PLoS Genet. *13*, e1006648. https://doi.org/10.1371/journal.pgen.1006648.

62. Burns, C.M., Chu, H., Rueter, S.M., Hutchinson, L.K., Canton, H., Sanders-Bush, E., and Emeson, R.B. (1997). Regulation of serotonin-2C receptor G-protein coupling by RNA editing. Nature *387*, 303–308. https://doi.org/10.1038/387303a0.

63. Niswender, C.M., Copeland, S.C., Herrick-Davis, K., Emeson, R.B., and Sanders-Bush, E. (1999). RNA Editing of the Human Serotonin 5-Hydroxytryptamine 2C Receptor Silences Constitutive Activity. J. Biol. Chem. *274*, 9472–9478. https://doi.org/10.1074/jbc.274.14.9472.

64. Abbas, A.I., Urban, D.J., Jensen, N.H., Farrell, M.S., Kroeze, W.K., Mieczkowski, P., Wang, Z., and Roth, B.L. (2010). Assessing serotonin receptor mRNA editing frequency by a novel ultra high-throughput sequencing method. Nucleic Acids Res. *38*, e118. https://doi.org/10.1093/nar/gkq107.

65. Gumpper, R.H., Fay, J.F., and Roth, B.L. (2022). Molecular insights into the regulation of constitutive activity by RNA editing of 5HT2C serotonin receptors. Cell Rep. *40*, 111211. https://doi.org/10.1016/j.celrep.2022.111211.

66. Niswender, C.M., Herrick-Davis, K., Dilley, G.E., Meltzer, H.Y., Overholser, J.C., Stockmeier, C.A., Emeson, R.B., and Sanders-Bush, E. (2001). RNA Editing of the Human Serotonin 5-HT2C Receptor: Alterations in Suicide and Implications for Serotonergic Pharmacotherapy. Neuropsychopharmacology *24*, 478–491. https://doi.org/10.1016/S0893-133X(00)00223-2.

67. Wheeler, E.C., Washburn, M.C., Major, F., Rusch, D.B., and Hundley, H.A. (2015). Noncoding regions of C. elegans mRNA undergo selective adenosine to inosine deamination and contain a small number of editing sites per transcript. RNA Biol. *12*, 162–174. https://doi.org/10.1080/15476286.2015.1017220.

68. Ingleby, L., Maloney, R., Jepson, J., Horn, R., and Reenan, R. (2009). Regulated RNA Editing and Functional Epistasis in Shaker Potassium Channels. J. Gen. Physiol. *133*, 17–27. https://doi.org/10.1085/jgp.200810133.

69. Nguyen, T.A., Heng, J.W.J., Kaewsapsak, P., Kok, E.P.L., Stanojević, D., Liu, H., Cardilla, A., Praditya, A., Yi, Z., Lin, M., et al. (2022). Direct identification of A-to-I editing sites with nanopore native RNA sequencing. Nat. Methods *19*, 833–844. https://doi.org/10.1038/s41592-022-01513-3.

70. Wenger, A.M., Peluso, P., Rowell, W.J., Chang, P.-C., Hall, R.J., Concepcion, G.T., Ebler, J., Fungtammasan, A., Kolesnikov, A., Olson, N.D., et al. (2019). Accurate circular consensus long-read sequencing improves variant detection and assembly of a human genome. Nat. Biotechnol. *37*, 1155–1162. https://doi.org/10.1038/s41587-019-0217-9.

71. Berg, S., Kutra, D., Kroeger, T., Straehle, C.N., Kausler, B.X., Haubold, C., Schiegg, M., Ales, J., Beier, T., Rudy, M., et al. (2019). ilastik: interactive machine learning for (bio)image analysis. Nat. Methods *16*, 1226–1232. https://doi.org/10.1038/s41592-019-0582-9.

72. Schindelin, J., Arganda-Carreras, I., Frise, E., Kaynig, V., Longair, M., Pietzsch, T., Preibisch, S., Rueden, C., Saalfeld, S., Schmid, B., et al. (2012). Fiji: an open-source platform for biological-image analysis. Nat. Methods *9*, 676–682. https://doi.org/10.1038/nmeth.2019.

73. Notredame, C., Higgins, D.G., and Heringa, J. (2000). T-coffee: a novel method for fast and accurate multiple sequence alignment 1 1Edited by. J. Mol. Biol. *302*, 205–217. https://doi.org/10.1006/jmbi.2000.4042.

74. Huang, J., Roberts, A.J., Leschziner, A.E., and Reck-Peterson, S.L. (2012). Lis1 Acts as a "Clutch" between the ATPase and Microtubule-Binding Domains of the Dynein Motor. Cell *150*, 975–986. https://doi.org/10.1016/j.cell.2012.07.022.

75. Roberts, A.J., Goodman, B.S., and Reck-Peterson, S.L. (2014). Reconstitution of dynein transport to the microtubule plus end by kinesin. Elife *3*, e02641. https://doi.org/10.7554/eLife.02641.

76. Bhabha, G., Cheng, H.-C., Zhang, N., Moeller, A., Liao, M., Speir, J.A., Cheng, Y., and Vale, R.D. (2014). Allosteric Communication in the Dynein Motor Domain. Cell *159*, 857–868. https://doi.org/10.1016/j.cell.2014.10.018.

77. Marzo, M.G., Griswold, J.M., and Markus, S.M. (2020). Pac1/LIS1 stabilizes an uninhibited conformation of dynein to coordinate its localization and activity. Nat. Cell Biol. *22*, 559–569. https://doi.org/10.1038/s41556-020-0492-1.

STAR★METHODS

KEY RESOURCES TABLE

REAGENT or RESOURCE	SOURCE	IDENTIFIER
Bacterial and virus strains		
E. coli BL21-CodonPlus(DE3)-RIPL	Agilent	Cat #230280
Biological samples		
Doryteuthis pealeii	Rosenthal lab – The Marine Biological Laboratory	N/A
Doryteuthis opalescens	egg casings collected off Scripps Pier, San Diego, CA	N/A
Chemicals, peptides, and recombinant proteins		
cOmplete EDTA-free protease inhibitor cocktail tablet	Roche	Cat #COEDTAF-RO
IgG Sepharose 6 fast flow beads	GE Healthcare	Cat #17-0969-01
Ni-NTA agarose	QIAGEN	Cat #30210
HaloTag TMR ligand	Promega	Cat #G8251
Deposited data		
Scripts for kymograph analysis	this paper	Github repository kjran/Kymo_analysis DOI:10.5281/zenodo.7699922
Scripts for pairwise correlation analysis	this paper	Github repository kjran/pairwise_corr_analysis DOI:10.5281/zenodo.7699924
Experimental models: Organisms/strains		
S. cerevisiae strains generated in this study	this paper	Table S6
Oligonucleotides		
Primers to amplify kinesin motor domain region from *D. opalescens* genomic DNA	this paper	Table S5
Recombinant DNA		
pET17b-K560	Vale et al.[18]	N/A
pET17b-DpealK554	this paper	N/A
pET17b-DopalK554	this paper	N/A
Software and algorithms		
Ilastik 1.3.3post3	Berg et al.[71]	www.ilastik.org
MATLAB R2021a Update 4	MathWorks (Natick, MA)	www.mathworks.com
Prism9	Graphpad (Boston, MA)	www.graphpad.com
Fiji (ImageJ)	Schindelin et al.[72]	imagej.net/software/fiji/downloads
OmicsBox (Blast2Go)	Biobam (Valencia, Spain)	www.biobam.com

RESOURCE AVAILABILITY

Lead contact

- Further information and requests for resources and reagents should be directed to and will be fulfilled by the lead contact, Samara L. Reck-Peterson (sreckpeterson@health.ucsd.edu)

Materials availability

- All plasmids generated in this paper will be shared by the lead contact upon request.

Data and code availability

- All data reported in this paper will be shared by the lead contact upon request.

- All original code has been deposited at Github and is publicly available as of the date of publication. DOIs are listed in the key resources table.
- Any additional information required to reanalyze the data reported in this paper is available from the lead contact upon request.

EXPERIMENTAL MODEL AND SUBJECT DETAILS

Animals

D. pealeii optic lobes and stellate ganglion were a gift from Joshua Rosenthal at The Marine Biological Laboratory. Specimens were collected by the animal collection department of the Marine Biological Laboratory in Woods Hole, MA during November of 2017. Stellate ganglion and optic lobe tissue were dissected by K.J.R. from each of three adult males and tissues were stored at −80°C. Because these animals were wild caught, their ages are unknown.

D. opalescens egg casings were collected by Phil Zerofski, head of marine collections at the Scripps Institute of Oceanography at UC San Diego off Scripps Pier, San Diego, CA in August of 2021. Water temperature at depth was 12–13°C. Egg casings were maintained in a seawater tank at 12–13°C. Newly hatched animals (less than 24 h old) were used in temperature experiments described in the method details below.

Yeast strains

S. cerevisiae strains used in this study are listed in Table S6. Cultures of *S. cerevisiae* for protein purification were grown and harvested as described in the method details below.

METHOD DETAILS

Mapping of edit sites

Edit sites and editing levels for *D. pealeii*, *S. officinalis*, *O. vulgaris*, and *O. bimaculoides*, *E. scolopes*, and *S. lineolata* were from previously reported RNA-seq data[5,7,8] and are tabulated in Tables S3 and S4. Alignments were performed using T-coffee multiple protein sequence alignments[73] to determine amino acid conservation at sites of cephalopod recoding. Cephalopod *DYNC1H1* homologues were aligned to *H. sapiens* (Uniprot: DYHC1_HUMAN), *M. musculus* (DYHC1_MOUSE), *S. cerevisiae* (DYHC_YEAST), *A. nidulans* (DYHC_EMENI), and *Doryteuthis melanogaster* (DYHC_DROME). Cephalopod *KINH* homologues were aligned to *H. sapiens* (KINH_HUMAN), *M. musculus* (KINH_MOUSE), and *D. melanogaster* (KINH_DROME).

Gene ontology (GO) term enrichment analysis

GO term enrichment analysis was performed using the Blast2GO toolkit in the OmicsBox suite (Biobam; Valencia, Spain). The *D. pealeii* transcriptome and list of edited proteins were previously reported.[5] p values were determined by Fisher's exact t-test.

Identification of recoding sites in the kinesin motor domain of *D. opalescens*

The sequence of the *D. opalescens* kinesin-1 motor domain (aa1-554) was determined from cDNA: a single animal was lysed and total RNA was extracted using the RNAeasy Plus extraction kit (Qiagen) as per the manufacturer's protocol. cDNA was generated using Accuscript High-fidelity first-strand cDNA synthesis kit (Agilent). The kinesin-1 motor domain was PCR amplified from cDNA using gene-specific primers based on the *D. pealeii* sequence (FW: CCTACTTTTGTTTGTGCGCG RV: TCTGCAGCATTTCCACCTACA).

To determine sites of RNA editing, we sequenced the kinesin-1 motor domain from genomic DNA and cDNA from the same individual animal cut in half at the collar as described below. Genomic DNA was extracted from the posterior portion of the animal using the DNAeasy extraction kit (Qiagen) following the manufacturer's protocol and RNA was extracted from the anterior portion using the RNAeasy Plus extraction kit.

To sequence the kinesin motor domain from genomic DNA, we used our cDNA sequence along with the *D. pealeii* genomic sequence as a guide to design a set of PCR primers to span predicted intron sequences. These primers are tabulated in Table S5, and the sequencing results are shown in Figure S3. The introns spanning exons 1 and 2 and exons 2 and 3 are 25,726 bp and 7,245 bp in *D. pealeii* respectively, and we were unable to amplify PCR products spanning these introns. Therefore, for these regions we designed primers based on the *D. pealeii* sequence to amplify the exons as well as the 5′ and 3′ intron-exon junctions for sequencing. For all other regions, we PCR amplified products spanning adjacent exons for sequencing the complete exons and 5′ and 3′ intron-exon junctions.

To determine sites of RNA editing, cDNA was generated from RNA extracted from the same individual animal using the Accuscript High-fidelity first-strand cDNA synthesis kit. The kinesin-1 motor domain was PCR amplified from cDNA using gene-specific primers (FW: CCTACTTTTGTTTGTGCGCG RV: TCTGCAGCATTTCCACCTACA) and cloned into the pCR-XL-2-TOPO vector (Invitrogen) as per the manufacturer's protocol. 87 individual clones were sequenced, and all A to G substitutions detected for each clone are shown in Figure S3. We identified 12 edit sites resulting in non-synonymous codon changes (ie. recoding sites) and 6 edit sites resulting in synonymous codon changes. These 12 recoding sites overlap with recoding sites previously reported in *D. pealeii*.[5,8] In addition to these 12 recoding sites, we detected two additional sites from our additional clone sequencing of *D. opalescens* at 6°C and 20°C

described below: we detected a single clone from an animal exposed to 6°C with an A to G substitution at nucleotide position 818 and a single clone from an animal exposed to 20°C with an A to G substitution at nucleotide position 1102. These two positions overlap with recoding sites previously reported in *D. pealeii* as well.

Strain generation

Yeast strain generation

All dynein constructs were generated in *S. cerevisiae* strain W303a. GST-Dyn1(331kDa)[42] was modified using PCR-based methods and transformed using the lithium acetate method. The following point mutations were generated using QuikChange site-directed mutagenesis (Agilent) and strains were verified by DNA sequencing: T2122A, N2915S, N3218D, N3218S., N3218G, I3272V, A3473T, K3455E, K3544R, K3544G, K3600R. See Table S6 for a list of yeast strains used in this study.

E. coli *strain generation*

All kinesin constructs were expressed in *E. coli* BL21-Codon Plus(DE3) (Agilent). All mutations were generated using QuikChange site-directed and multi-site directed mutagenesis (Agilent) and all constructs were verified by DNA sequencing. Human K560-GFP was a gift from the Vale lab. The following point mutations were generated in human K560-GFP: K67E, K67R, K67G, Y77C, N117D, N117S, N117G, K166E, K281R, and R367K. To generate unedited *D. pealeii* K554-GFP, the first 554 amino acids of *D. pealeii* KINH was determined from the *D. pealeii* transcriptome,[7] synthesized as a codon-optimized gene block (IDT), and cloned into pET17b. The following mutation variants were generated in *D. pealeii* unedited K554-GFP: OL-1: S75G, Y77C, N117G, K368R, K479R, K483R; SG-1: S75G, Y77C, N117D, K368R, K479R, K483G, E515G; SG-2: K368R, K479R, K483R. The *D. opalescens* kinesin-1 motor domain sequence was determined as described above and *D. opalescens* K554-GFP was generated in pET17b. The following mutation variants were generated in *D. opalescens* unedited K554-GFP: Cold-1: S75G, Y77C, K368R, K483R; Cold-2: S75G, Y77C, N117D, K368R, K483R; Cold-3: K67R, Y77C, N117D, K368R, K479R, K483G, E515G.

Protein purification

Dynein constructs

Cultures of *S. cerevisiae* for protein purification were grown, harvested, frozen and purified as described previously.[42] Yeast cells were grown to an OD_{600} of 2–3. Cells were harvested by centrifugation, washed once with water, then frozen by drops in liquid nitrogen. Liquid nitrogen-frozen yeast cell pellets were lysed by grinding with a chilled coffee grinder and resuspending in dynein lysis buffer (DLB: final concentration 30 mM HEPES [pH 7.4], 50 mM potassium acetate, 2 mM magnesium acetate, 1 mM EGTA, 10% glycerol, 1 mM DTT) supplemented with 0.1 mM Mg-ATP, 0.5 mM Pefabloc, 0.05% Triton and cOmplete EDTA-free protease inhibitor cocktail tablet (Roche)). The lysate was clarified by centrifuging at 264,900 × g for 1 h at 4°C. The clarified supernatant was incubated with IgG Sepharose beads (GE Healthcare Life Sciences) for 1.5 h at 4°C. The beads were transferred to a gravity flow column, washed with DLB buffer supplemented with 250 mM potassium chloride, 0.1 mM Mg-ATP, 0.5 mM Pefabloc and 0.1% Triton, and with TEV buffer (10 mM Tris–HCl [pH 8.0], 150 mM potassium chloride, 10% glycerol, 1 mM DTT, 0.1 mM Mg-ATP and 0.5 mM Pefabloc). Constructs were labeled with 5 μM Halo-TMR (Promega) in the column for 10 min at room temperature and unbound dyes were washed with TEV buffer at 4°C. Dynein was cleaved from IgG beads via incubation with 0.15 mg/mL TEV protease for 1 h at 16°C. Cleaved proteins were filtered by centrifuging with Ultra-free-MC VV filter (EMD Millipore) in a tabletop centrifuge at 4°C, flash frozen in liquid nitrogen and stored at −80°C.

Kinesin constructs

Human K560-GFP and squid K554-GFP constructs were purified from BL21-CodonPlus(DE3)-RIPL (Agilent) *E. coli*. Cultures were grown to OD 0.6–0.8 and expression was induced with 0.75 mM IPTG for 16 h at 18°C. Cultures were pelleted, washed in PBS, and then frozen in liquid nitrogen. Frozen pellets were resuspended in lysis buffer (50 mM Tris [pH 7.5], 250 mM sodium chloride, 1 mM magnesium chloride, 20 mM imidazole [pH 7.4]) supplemented with 0.5 mM Mg-ATP, 10 mM beta-mercaptoethanol, 1 mM Pefabloc, cOmplete EDTA-free protease inhibitor cocktail tablet (Roche) and 50 mg/mL lysozyme) and kept on ice for 30 min. Cultures were lysed by sonicating at 50% power for 30 cycles with 5 s pulses and 20 s of rest on ice. Lysates were clarified by centrifuging at 92,600 × g for 30 min at 4°C. The clarified supernatant was incubated with Ni-NTA agarose beads (Qiagen) for 1 h at 4°C. The beads were transferred to a gravity flow column, washed with lysis buffer supplemented with 0.5 mM Mg-ATP, 10 mM beta-mercaptoethanol, and 1 mM Pefabloc, then eluted with elution buffer (50 mM Tris [pH 7.5], 250 mM sodium chloride, 1 mM magnesium chloride, 250 mM imidazole [pH 7.4]) supplemented with 0.1 mM Mg-ATP, and 10 mM beta-mercaptoethanol. Eluants were then desalted using a PD-10 column (GE Healthcare) and buffer exchanged into BRB80 (80 mM K + PIPES[pH 6.8], 2 mM magnesium chloride, 1 mM EGTA) supplemented with 0.1 mM Mg-ATP and 0.1 mM DTT. Sucrose was added to the elution to a final concentration of 10%, and eluants were flash frozen in liquid nitrogen and stored at −80°C.

TIRF microscopy

Imaging was performed with an inverted microscope (Nikon, Ti-E Eclipse) equipped with a 100 × 1.49 N.A. oil immersion objective (Nikon, Plano Apo). The xy position of the stage was controlled by a Pro-Scan linear motor stage controller (Prior). The microscope was equipped with a MLC400B laser launch (Agilent), with 405 nm, 488 nm, 561 nm and 640 nm laser lines. The excitation and emission paths were filtered using appropriate single bandpass filter cubes (Chroma). The emitted signals were detected with an electron multiplying CCD camera (Andor Technology, iXon Ultra 888). Illumination and image acquisition was controlled by NIS Elements

Advanced Research software (Nikon). Temperature-controlled motility assays were performed using a Linkam PE100-NIF inverted Peltier stage and T96 System Controller. Flow chamber slides were covered with a custom copper-plated aluminum fitting and empirical temperature of the flow chamber was monitored using a Type K thermocouple sensor probe.

Motility assays

Single-molecule motility assays were performed in flow chambers made with double-sided tape using the TIRF microscopy set-up described above. No. 1–1/2 coverslips (Corning) were used for the flow chamber assembly and sonicated in 100% ethanol for 10 min to reduce non-specific protein binding. Taxol-stabilized microtubules with ~10% biotin-tubulin and either ~10% Alexa 488-tubulin or Alexa 405-tubulin were attached to the flow chamber via biotin-BSA and streptavidin as described previously.[74] For each frame, kinesin-GFP and TMR-dynein were exposed for 100 ms with the 488 nm laser and 561 nm laser, respectively.

For motility assays, a final concentration of 2.5–5 pM of dynein or 50–500 pM of kinesin was flowed into the flow chamber pre-assembled with taxol-stabilized microtubules. Motor concentrations used were empirically determined to optimize the number of runs per kymograph. The final imaging buffer contained DLB (30 mM HEPES [pH 7.4], 2 mM magnesium acetate, 1 mM EGTA, 10% glycerol, 50 mM potassium acetate), 20 μM taxol, 1 mM Mg-ATP, 1 mg/mL casein, 1 mM DTT, 71.5 mM β-mercaptoethanol and an oxygen scavenger system (0.4% glucose, 45 μg/mL glucose catalase, and 1.15 mg/mL glucose oxidase). Microtubules were imaged first by taking a single-frame snapshot. Dynein was imaged every 500 ms for 5 min, and kinesin was imaged every 200 ms for 1 min. At the end, microtubules were imaged again by taking a snapshot to check for stage drift and images showing drift were omitted from analysis. Dynein was imaged for no longer than 20 min, and kinesin was imaged for no longer than 10 min. For motility assays performed at 25°C and 8°C, slides were equilibrated on the Peltier stage for 1.5 min before imaging and temperature was monitored immediately before and after imaging using a thermocouple probe.

Kymograph analysis

Motility movies were analyzed using the analysis workflow outlined in Figure S1. First, kymographs were generated using an ImageJ macro as previously described.[75] Kymographs were then pixel classified using Ilastik 1.3.3post3,[71] and pixel-classified images were analyzed with custom MATLAB scripts (MATLAB R2021a Update 4). Individual runs were parsed from the skeletonized images and velocity and run distance measurements were determined. Runs shorter than 4 frames were excluded from analysis. Processive runs were defined as any run with a velocity of 15 nm/s or greater. Because motor velocity can change throughout a run, velocity measurements reflect segment velocities. Segments were defined using the findchangepts function to detect changes in run mean and slope. Landing rates for each kymograph were calculated as total number of events (motile + non-motile)/μm of microtubule length. See below for statistical analysis.

Determination of edit site combinations from *D. pealeii* tissues

Stellate ganglion and optic lobes were lysed and total RNA was extracted using the RNAeasy Plus extraction kit. cDNA was generated using Accuscript High-fidelity first-strand cDNA synthesis kit. The kinesin-1 motor domain was PCR amplified from cDNA using gene-specific primers (FW: CCTACTTTTGTTTGTGCGCG RV: TCTGCAGCATTTCCACCTACA) and cloned into the pCR-XL-2-TOPO vector. Individual clones were selected and sequenced to determine edit site combinations of individual transcripts. For each dataset, three samples were processed and 100 clones for each sample were sequenced. Sequences with incomplete or low-quality sequencing for any portion of the motor domain were omitted and data were pooled per condition. See below for statistical analysis.

D. opalescens temperature experiment

D. opalescens egg cases were collected off the Scripps Pier in San Diego, CA. Water temperature at depth was 12–13°C. Egg casings were transferred to a seawater tank maintained at 12–13°C. Tanks were monitored for temperature stability. Newly hatched animals (less than 24 h old) were transferred to tanks maintained at 6°C, 8°C, 12°C, 16°C, or 20°C and held at these temperatures for 24 h. Animals were then flash frozen in liquid nitrogen and stored at −80°C.

Determination of editing levels and edit site combinations in *D. opalescens*

RNA extraction, cDNA synthesis, and PCR amplification of kinesin was performed as described above for *D. pealeii* with the same primer set as above for 10 animals from each temperature. PCR products were then directly sequenced using reverse primers, and percent editing at each recoding site was determined by peak height analysis calculated by (C peak height)/(C + T peak heights). Only high quality, complete sequencing data was used for percent editing analysis.

Edit site combinations in *D. opalescens* were determined for three animals exposed to 6°C water, and three animals exposed to 20°C water as described above for *D. pealeii.*

QUANTIFICATION AND STATISTICAL ANALYSIS

Statistical analysis of motility assays

All statistical analyses were determined using Prism9 (GraphPad). For velocity measurements, mean velocities were determined by fitting velocity histograms to a Gaussian distribution. Mean, Standard error of the mean (SE), 95% Confidence intervals of the mean,

Goodness of fit (R^2), and the degrees of freedom (dF) for each fit are reported in Table S2 and p values were calculated by two-tailed t-test comparing the best-fit mean values. For run distance measurements, mean decay constants (tau) were determined by fitting 1-cumulative frequency distributions to a one-phase exponential decay. Tau, 95% Confidence intervals of tau, K (rate constant), Standard error of K (SE), Goodness of fit (R^2), and the degrees of freedom (dF) for each fit are reported in Table S2 and p values were calculated by two-tailed t-test comparing the best-fit values for the rate constant K. For all velocity and run distance data, n is the number of measurements pooled from at least two independent protein preparations. For percent processivity measurements, p values were determined by two-tailed t-test. For landing rate measurements, p values were determined by two-tailed t-test with Welch's correction. All fits and p values are tabulated in Table S2.

Statistical analysis of combinatorial editing

Correlation analysis of recoding sites was performed as follows using a custom MATLAB script: The observed instances of each recoding site pair were compared against all possible outcomes for each pair given the number of transcripts sequenced. The p value for each pairwise comparison was determined by calculating the probability of observing a more rare scenario given the null hypothesis that transcript sequences are independent of one another and recoding at each site along a transcript occurs independently at the observed frequency. All p values are tabulated in Table S2.

Statistical analysis of editing levels per site between 6°C and 20°C

For Figure 3C, significance was determined by Mann-Whitney test comparing ranks and corrected for multiple comparisons by determining the false discovery rate (FDR) through the corrected FDR method of Benjamini and Yekutieli (Desired FDR (Q) of 1.00%). For Figure S4I, significance was determined by Fisher's exact test. All p values are tabulated in Table S2.

CellPress
OPEN ACCESS

Supplemental figures

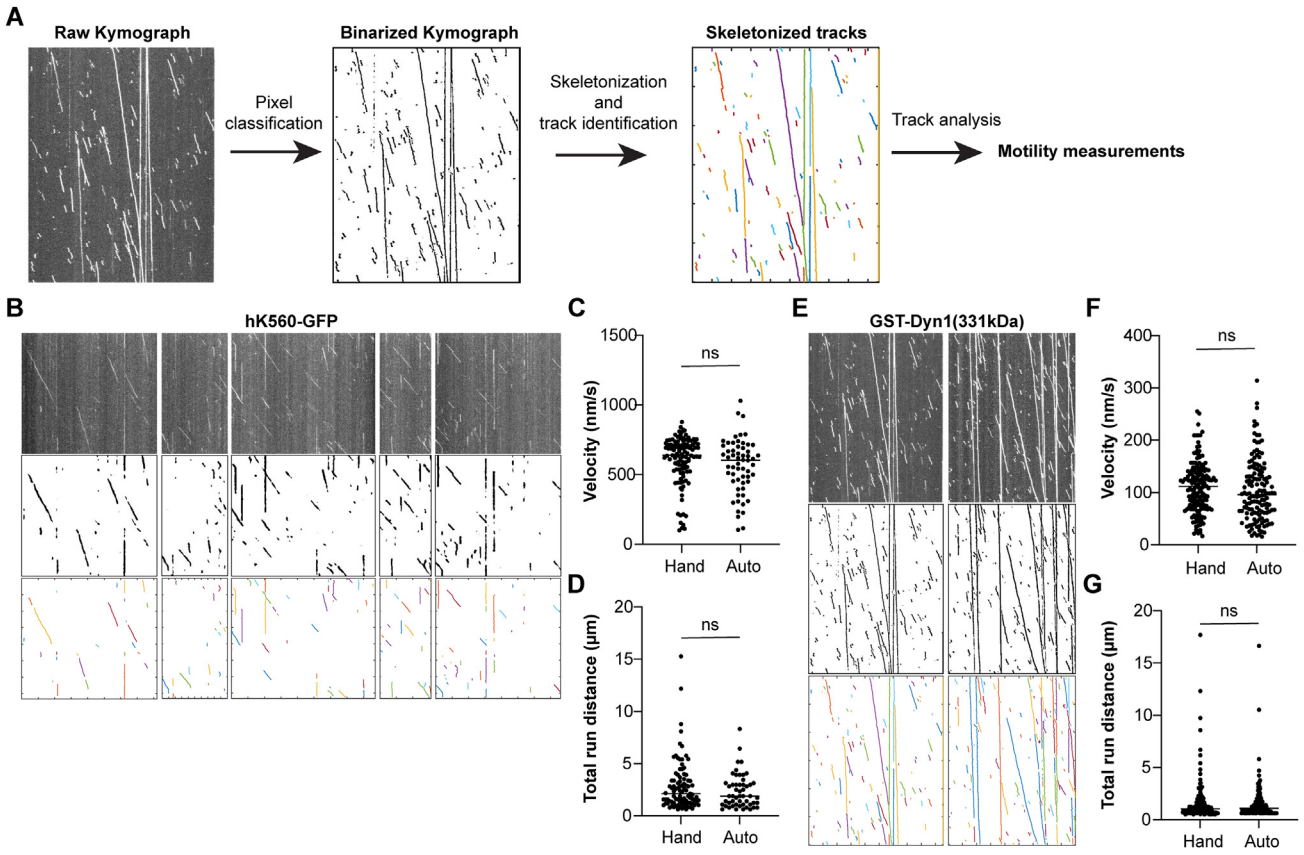

Figure S1. Comparison of automated kymograph analysis with hand-tracked kymograph analysis, related to Figures 2, 4, and 6

(A) Automated kymograph analysis workflow. See STAR Methods for details.

(B) Kymographs of human kinesin (K560) alongside pixel-classified and skeletonized kymograph images. These kymographs were used to compare hand-tracking vs. automated tracking in (C and D).

(C) Individual velocity measurements (nm/s) of human kinesin as determined by hand-tracking vs. automated tracking.

(D) Individual run distance measurements (µm) of human kinesin as determined by hand-tracking vs. automated tracking.

(E) Kymographs of yeast dynein (GST-Dyn1(331kDa)) alongside pixel-classified and skeletonized kymograph images. These kymographs were used to compare hand-tracking vs. automated tracking in (F and G).

(F) Individual velocity measurements (nm/s) of yeast dynein as determined by hand-tracking vs. automated tracking.

(G) Individual run distance measurements (µm) of yeast dynein as determined by hand-tracking vs. automated tracking.

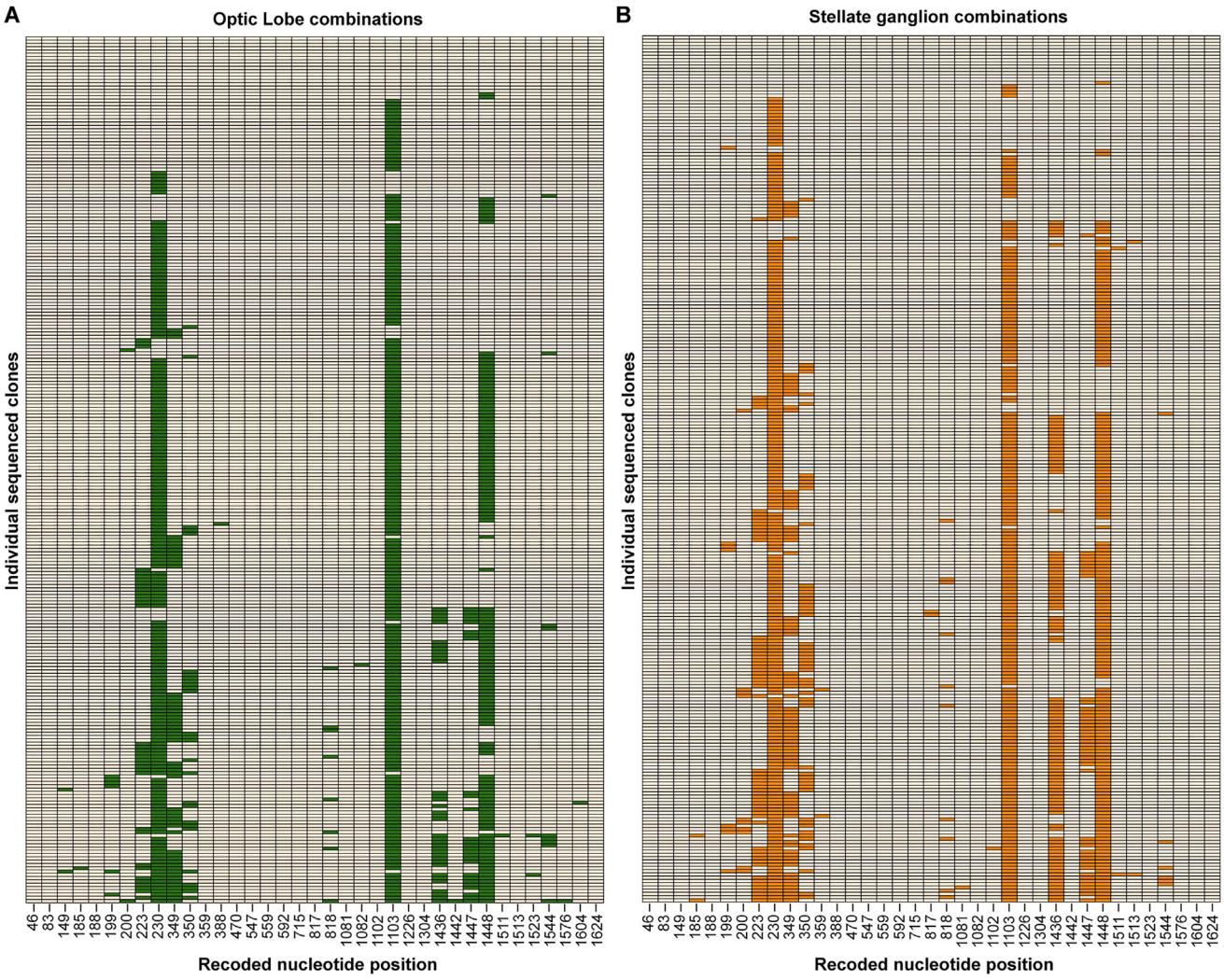

Figure S2. Tissue-specific recoding of the kinesin motor domain in *D. pealeii*, related to Figure 2

(A and B) All recoding site combinations detected from the optic lobe (A) and the stellate ganglion (B) of *D. pealeii.*

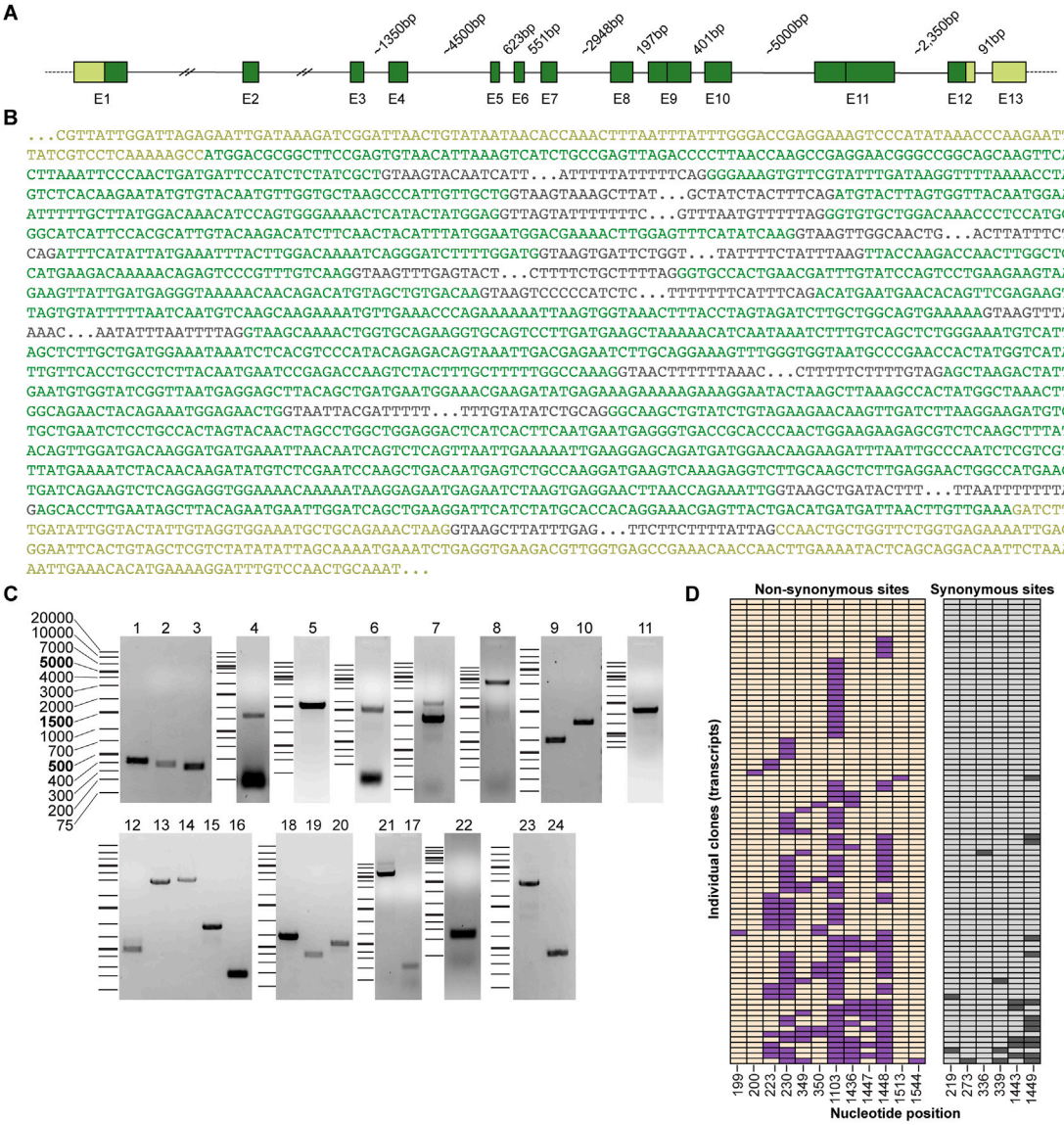

Figure S3. Identification of recoding sites in the kinesin motor domain of *D. opalescens*, related to Figure 3

(A) Exon structure of the kinesin motor domain from *D. opalescens*. See STAR Methods for details. Coding sequence for the kinesin motor domain (amino acids 1–554) is indicated in dark green and spans 12 exons. All exon sequences and intron-exon junctions in the coding sequence were sequenced. All 5′ and-3′ intron junctions are canonical. Exact intron sizes are indicated when determined from sequencing through the entire intron. Estimated intron sizes are indicated with a tilde and were determined based on PCR product sizes from PCRs performed using *D. opalescens* genomic DNA as a template.

(B) Sequence of the exons and exon junctions of the *D. opalescens* kinesin motor domain.

(C) PCR products from primer sets in Table S5 yielding the genomic sequence of the *D. opalescens* kinesin motor domain. Ladders were run in each gel but are cropped out for space.

(D) Clone sequencing of the kinesin motor domain from cDNA generated from the same individual animal used for genomic DNA sequencing shown. We sequenced 87 clones and detected 12 non-synonymous edit sites and 6 synonymous edit sites. Nucleotide position is with reference to the start codon A as 1. All of the edit sites detected (excepting a single synonymous edit detected at position 273) were previously reported in *D. pealeii*. As described in the methods, we detected two additional recoding sites from our clone sequencing of *D. opalescens* at 6°C and 20°C: a single clone from an animal exposed to 6°C with an A to G substitution at nucleotide position 818 and a single clone from an animal exposed to 20°C with an A to G substitution at nucleotide position 1102 (see Figures S4A and S4B). These two positions are reported sites of recoding in *D. pealeii* and were included in Figure 3.

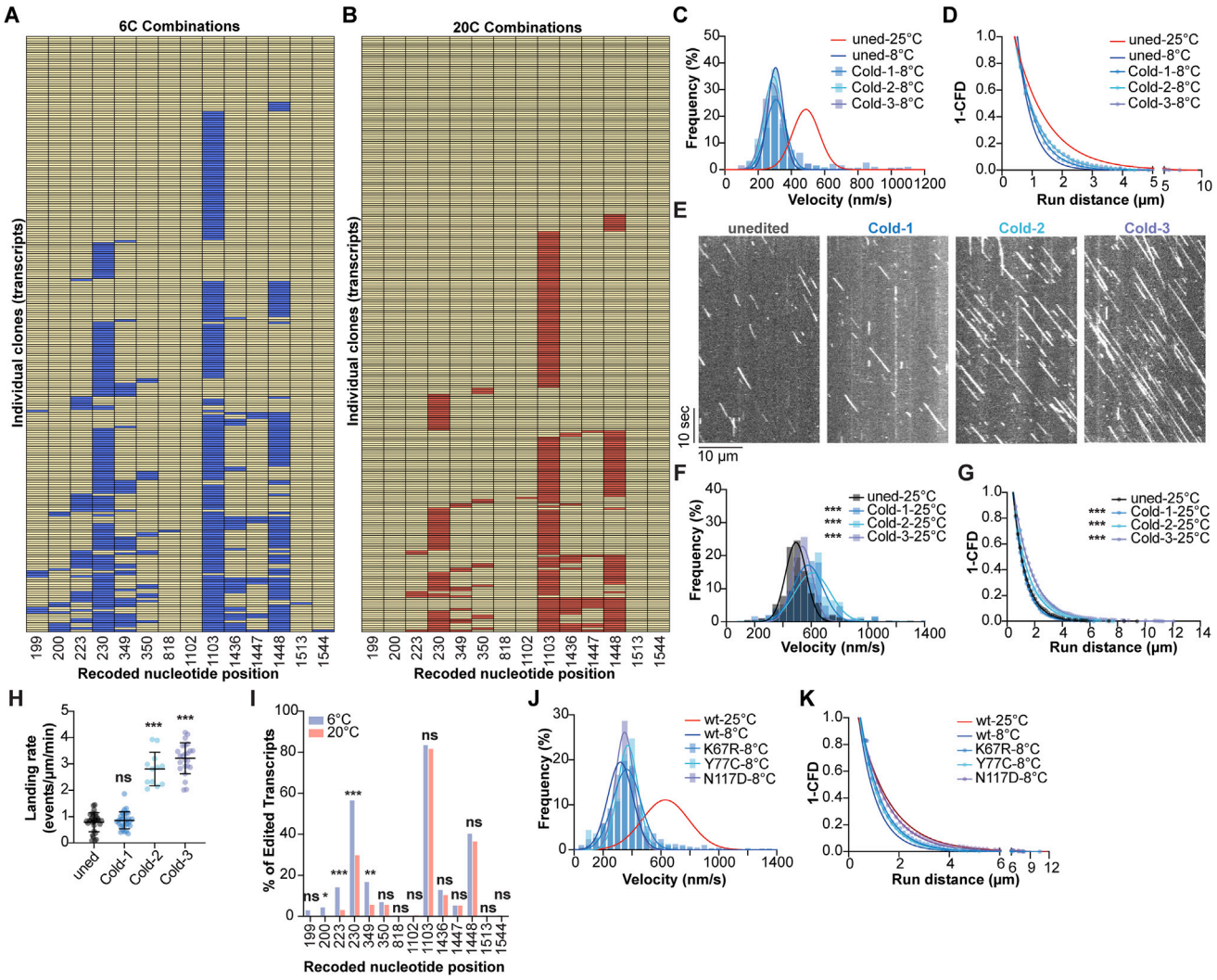

Figure S4. Frequency and motility of cold-specific kinesin variants and substitutions, related to Figure 4

(A and B) All recoding site combinations detected from *D. opalescens* exposed to 6°C water (A) and 20°C water (B).

(C and D) Velocity histograms (C) and 1-CFD plots (D) of cold-specific kinesin variants shown in Figures 4D–4G.

(E) Representative kymographs of unedited *D. opalescens* kinesin and variants Cold-1, Cold-2 and Cold-3 at 25°C.

(F) Velocity analysis of unedited *D. opalescens* kinesin and variants Cold-1, Cold-2 and Cold-3 at 25°C.

(G) Run distance analysis of unedited *D. opalescens* kinesin and variants Cold-1, Cold-2 and Cold-3 at 25°C.

(H) Landing rates of unedited *D. opalescens* kinesin and variants Cold-1, Cold-2 and Cold-3 at 25°C.

(I) Percent of edited transcripts that are recoded at the indicated nucleotide position in *D. opalescens* at 6°C compared to 20°C. Significance was calculated by Fisher's exact test.

(J and K) Velocity histograms (J) and 1-CFD plots (K) of cold-preferred substitutions shown in Figures 4H–4K.

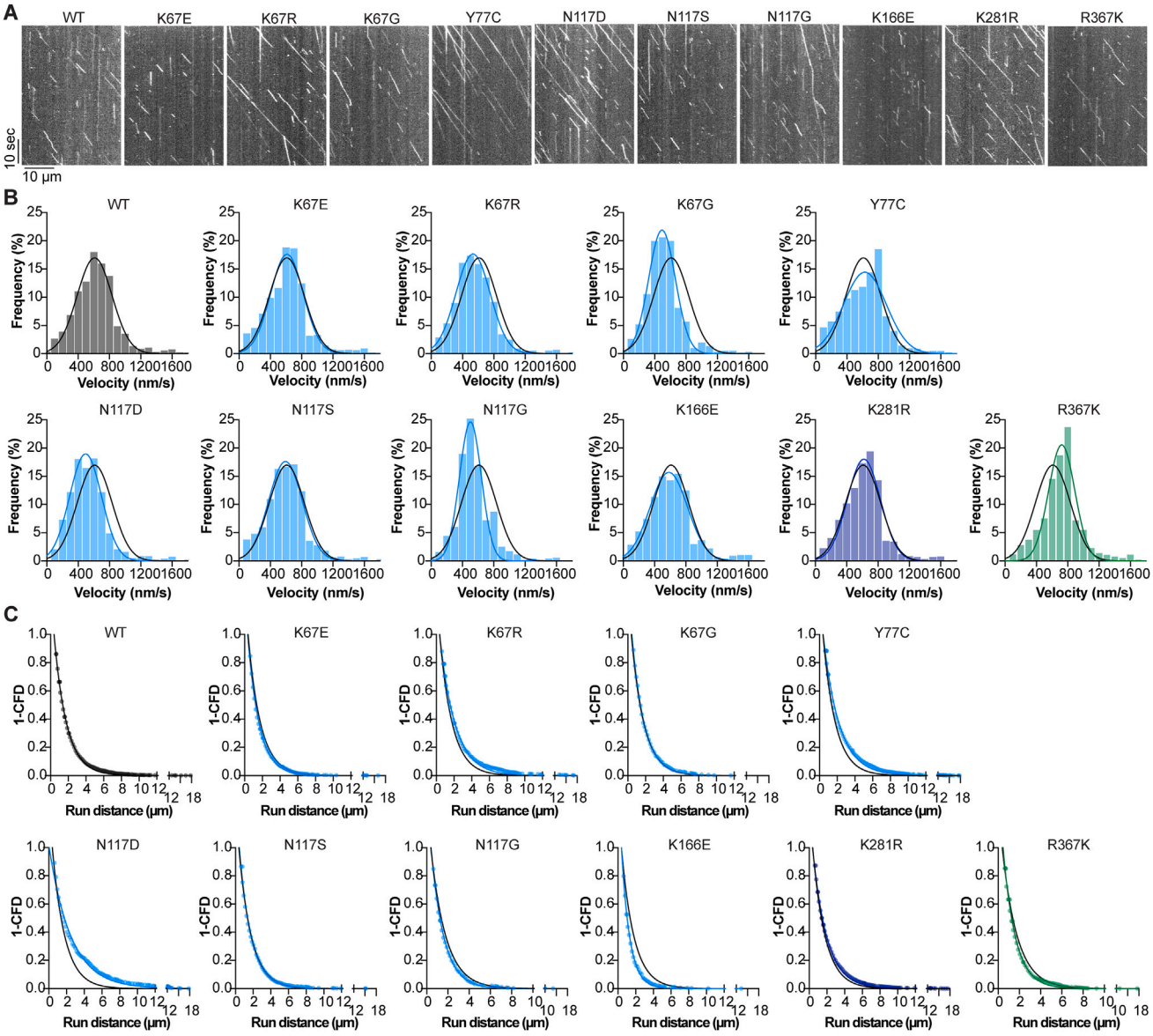

Figure S5. Motility of human kinesin mutants, related to Figure 6

(A–C) Representative kymographs (A), velocity frequency distributions (B), and run distance frequency distributions (C) for each human kinesin mutant shown in Figure 6. Substitutions not discussed in the main text are discussed here:

Arg367 is located in the neck coiled coil. Humans encode an arginine at this position, while cephalopods encode a lysine. An Arg367Lys substitution in human kinesin resulted in increased velocity and decreased run distance.

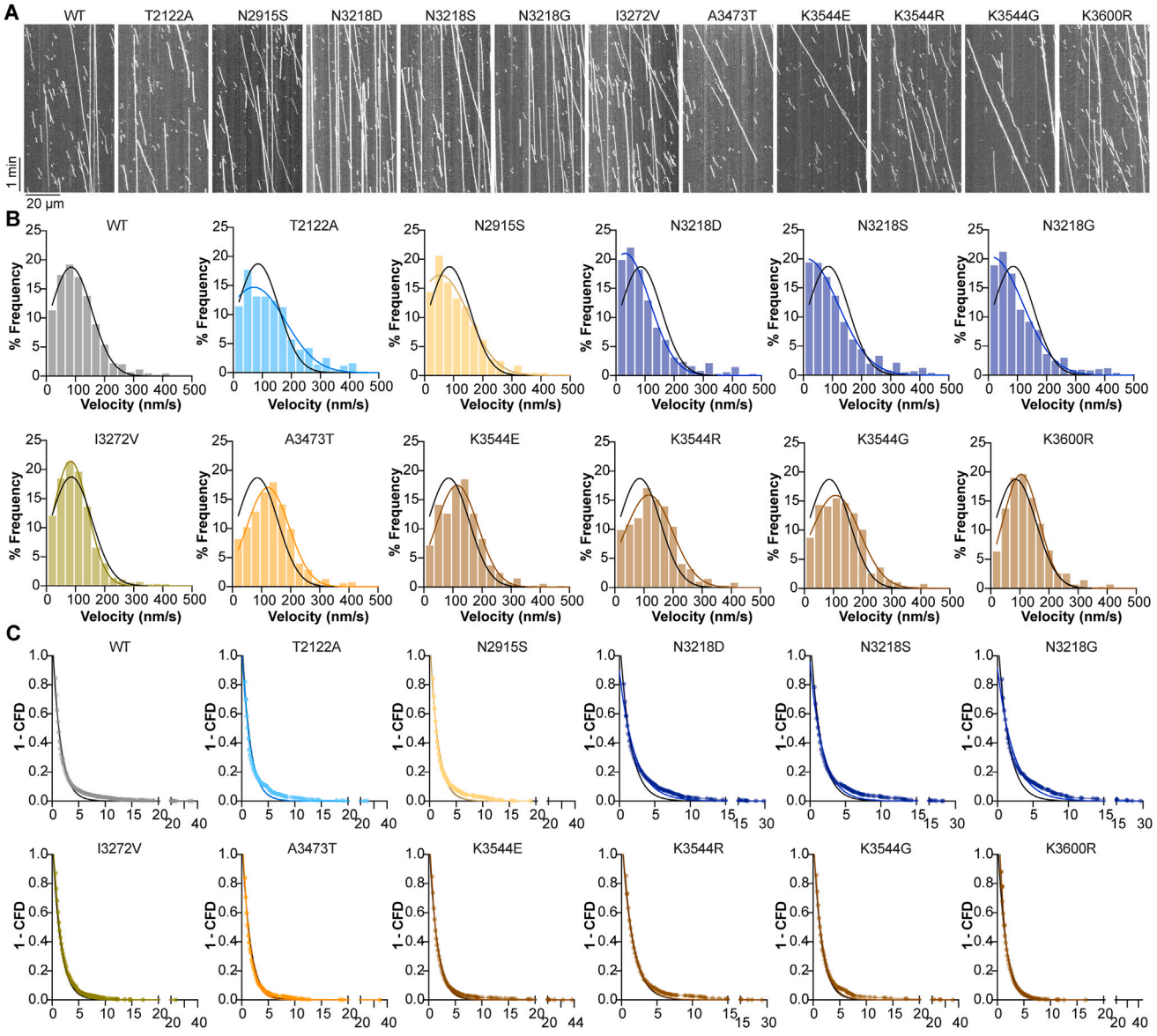

Figure S6. Motility of yeast dynein mutants, related to Figure 6

(A–C) Representative kymographs (A), velocity frequency distributions (B), and run distance frequency distributions (C) for each yeast dynein mutant shown in Figure 6. Substitutions not discussed in the main text are discussed here:

Thr2122 is located within the H2 insert loop in AAA2L that contacts the linker when the linker bends upon ATP binding at AAA1 and ring closure.[32] A triple mutant of this contact region containing T2122G in yeast GST-Dyn1(331kDa) displays decreased velocity in single molecule motility assays[76] and deletion of the entire H2 insert region in *Dictyostelium* dynein results in lower microtubule-stimulated ATPase activity.[30] We found that Thr2122Ala did not significantly affect velocity or run distance. However, multiple amino acids in the H2 hairpin insert are recoded in cuttlefish (hTyr2265 (recoded to Cys), hAsn2271 (recoded to Ser), hThr2272 (recoded to Ala)) and it is possible that these substitutions may affect linker docking at AAA2 in other assays or when occurring in combination with each other.

Asn2915 is located at the edge of AAA4L near the AAA3/4 interface. Asn2915Ser modestly decreased velocity without altering run distance.

Ile3272 is located in the stalk and is an important stalk/stalk contact site for stabilizing the autoinhibited Phi form of dynein.[33] An Ile3272Ala mutation in full-length yeast dynein results in increased run distance and decreased velocity.[77] We found that Ile3272Val in GST-Dyn1(331kDa) did not significantly affect velocity or run distance.

Ala3473: Humans encode a threonine at this position while *Saccharomyces cerevisiae* encodes an alanine. Cephalopods encode a threonine at this position but can edit it to an alanine. We found that Ala3473Thr increased velocity and decreased run distance. Ala3473 lies at the edge of an exposed loop within AAA5L that is near contact sites between AAA5 and the linker.[31] Interestingly, a known contact site between AAA5 and the linker is also a cuttlefish recoding site (hLys3621 (recoded to Arg)) as is the adjacent residue (hAsn3622 (recoded to Asp)). Mutation of linker contact sites in AAA5 decreases single molecule velocity of GST-Dyn1(331kDa).[31] Another residue (yArg3476) lies on the opposite side of the AAA5 loop containing Ala3473 and may be involved in stabilizing electrostatic interactions between AAA5/AAA5 domains in the Phi conformation; a Arg3476Asp mutation in full-length yeast dynein results in increased run distance.[77]